Atmospheric Environment 318 (2024) 120267

Contents lists available at ScienceDirect

Atmospheric Environment

journal homepage: www.elsevier.com/locate/atmosenv

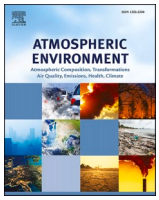

Characterization of urban aerosol pollution before and during the COVID-19 crisis in a central-eastern European urban environment

Zsófia Kertész [a,*], Shafa Aljboor [a,b], Anikó Angyal [a], Enikő Papp [a], Enikő Furu [a], Máté Szarka [a], Sándor Bán [a], Zita Szikszai [a]

[a] HUN-REN Institute for Nuclear Research (ATOMKI), Debrecen, Hungary
[b] University of Debrecen, Ph.D. School in Physics, Debrecen, Hungary

HIGHLIGHTS

- Characterization of urban air pollutants during 4 lockdowns and 2 relaxation periods
- A 20% reduction of PM and gaseous pollutants in average in the 2 years of COVID-19
- Variation of concentration, composition, and sources of $PM_{2.5}$ and PM_{coarse}
- Introduction of an integrated approach combining receptor modelling, trajectory statistical methods and local meteorology
- Impact of long-range transport, meteorology and the change of emission in source regions is determined

ARTICLE INFO

Keywords:
Urban aerosol pollution
Elemental composition
Source apportionment
COVID-19 lockdowns & relaxation periods

ABSTRACT

The worldwide restrictions due to the COVID-19 pandemic induced a radical change in urban air quality. The objective of this work was to study and understand the variation of PM_{coarse} and $PM_{2.5}$ pollution besides other air quality (AQ) parameters in the city of Debrecen, Hungary from 2018 to 2022. To achieve this goal, we introduced an integrated approach that combines source apportionment by receptor modelling, trajectory-based statistical methods and takes into account local and regional meteorology. Concentration, elemental composition, and sources of atmospheric particulate matter (APM) were determined for four lockdown periods with varying levels of restrictions, two transition intervals and two relaxation periods in 2020-22, and they were compared to corresponding baseline values from 2018-19. The concentration, composition and sources of $PM_{2.5}$, PM_{coarse} showed strong seasonality. The main component of PM_{coarse} was mineral dust (32%), while BC (15%), sulphate aerosols (19%) and mineral dust (13%) were the major constituents of $PM_{2.5}$. Source apportionment by Positive Matrix Factorization identified 8 sources on both size fractions: two types of soil, traffic, combustions, biomass burning, biogenic emission, sea salt, construction, roadworks, secondary sulphate. The relative contribution of sources did not change during the pandemic compared to the previous two years. However, considering the whole 2-year-long period affected by restrictions, a 20–25% reduction was detected in the concentrations and source contributions, apart from temporary sources like roadworks or sea salt episodes. The changed habits of the population could be traced in the evolution of APM. Before the pandemic, increased concentration of traffic related pollutants was characteristic of the school year, while in 2020-21 it was more typical in the summers, the relaxation periods. On the other hand, staying at home during lockdowns led to a significant increase in biomass burning from domestic heating in spring 2020 and 2021. By studying the individual lockdown and relaxation periods, we have shown that the evolution of APM pollution in relatively short, 2-3-month intervals was significantly influenced by local and regional meteorological parameters, the origin of air masses, desert dust episodes and periodic construction works.

* Corresponding author. ATOMKI, H-4026, Debrecen, Bem tér 18/c, Hungary.
E-mail address: kertesz.zsofia@atomki.hu (Z. Kertész).

https://doi.org/10.1016/j.atmosenv.2023.120267
Received 29 September 2023; Received in revised form 23 November 2023; Accepted 27 November 2023
Available online 4 December 2023

1. Introduction

Atmospheric aerosols have significant effects on many aspects of our lives. They affect the Earth's climate as strongly as greenhouse gases, and they influence the weather as well. Aerosols may also reduce visibility, which in many parts of the world results in haze. Aerosols have a considerable impact on the biosphere and the natural and built environments, too.

Air pollution, especially particulate matter (PM) pollution, causes the premature death of over 4 million people each year (Pérez Velasco and Jarosińska, 2022). PM pollution is linked to several health problems like lung cancer, chronic obstructive pulmonary (COPD), heart disease, and stroke (Manisalidis et al., 2020).

The COVID-19 pandemic caused by the coronavirus SARS-CoV-2 emerged at the end of 2019 and became a world pandemic in early 2020. The COVID-19 pandemic reached almost every country in the world. The outbreak of the pandemic forced most governments to establish strict regulations in their countries to stop the virus's spread. Hungary was no exception. In order to establish social distance, a nationwide lockdown was imposed in Hungary on March 12, 2020. Schools and institutions were closed, non-essential business and industrial activities were restricted, all public and sporting events were cancelled, the country's borders were closed, and curfew was in force from 8 p.m. to 5 a.m. The restrictions were gradually eased from May 4, 2020. In the following two years, different levels of restrictions were in force from time to time, depending on the evolution of the epidemiological situation (AboutHungary, n.d.).

Shutdowns and restrictions around the world provided a precious window for researchers to study changes in urban aerosol pollution under conditions of reduced anthropogenic activities. Several studies have been published that deal with the changes in air quality during the lockdown (Bakola et al., 2022; Bao and Zhang, 2020; Berman and Ebisu, 2020; Briz-Redón et al., 2021; Higham et al., 2021; Menut et al., 2020; Nakada and Urban, 2020; Vadrevu et al., 2020). The first investigations were based on data from regulatory monitoring networks. They revealed that there was a considerable reduction in atmospheric pollutants and an improvement in air quality compared to the pre-lockdown period (Bakola et al., 2022; Ghahremanloo et al., 2021; Putaud et al., 2023; Sokhi et al., 2021). For example, in the case of PM_{10} the reduction varied between 5% (North America) and 42% (South Asia). In Europe, the decrease was 17%. $PM_{2.5}$ showed similar tendencies, i.e., a 20% decrease in Europe, over 40% in Asia, and less than 10% in North America. Concentration of NO_2, which is closely related to vehicle emission, was decreased by 18–60%, over 40% in Europe. In Budapest, Hungary, similar tendencies were observed for the first lockdown period in spring, 2020 at traffic sites (Salma et al., 2020b; Varga-Balogh et al., 2021). However, during this first lockdown period in Hungary, the reduction of air pollution was not so marked in the suburban sites of Budapest and in other cities as well. In addition, PM_{10} concentrations showed no decrease at all in the majority of the cities. This lack of reduction in PM concentration was explained by the meteorological conditions.

More recently, a limited number of studies are available on the composition and sources of PM pollution during the COVID-19 lockdown (Clemente et al., 2022; Gamelas et al., 2023; Giardi et al., 2022; Jeong et al., 2022; Manchanda et al., 2021), but only a few are related to middle Europe (Ivanovski et al., 2022; Rys et al., 2022) and none to Hungary. In addition, most of these works report results only from the first lockdown period in early 2020. These studies report significant decrease in the concentration of traffic related components and source contributions, while the behavior of secondary aerosols showed a mixed picture (Massimi et al., 2022).

In this work, we characterize the $PM_{2.5}$, PM_{coarse}, and PM_{10} pollution at an urban background site in Debrecen, Hungary, for 4 years between March 2018 and February 2022. This period covers the whole 2 years affected by the COVID-19 pandemic (March 2020–February 2022), which gives us a more complete picture of the effects of societal responses to the pandemic. Air pollution during the four lockdown periods corresponding to the four waves of the pandemic with different restriction measures and the two relaxation periods was also compared. Given the complexity of the problem, an integrated approach combining source apportionment by positive matrix factorization (PMF), trajectory statistical methods and local and regional meteorology was applied. On this basis, the influence of local and regional sources was assessed before and during COVID, too. We also determined which parameters other than anthropogenic activity influenced the evolution of air pollution levels.

2. Methods

2.1. Sampling location

Debrecen is the second-largest city in Hungary, with approx. 200 000 inhabitants. The city is an educational, scientific, and cultural center, surrounded by forests and agricultural areas. The city lies on the border of two regions: the sandy region of Nyírség and the loess area of Hajdúság, (Pásztor et al., 2018). The climate of the city is predominantly dry continental with periodic oceanic and Mediterranean influence (OMSZ, n.d.-a). The prevailing wind direction is N, NW, NE. The industrial activity was modest at the time of the investigation. At the end of 2019 a large-scale development of the northern industrial park has begun on 400 ha preparing for the installation of a new BMW factory, which is the largest industrial investment in the area in the last 30 years. The construction of the infrastructure was suspended in May 2020 due to the pandemic and restarted in the 3rd quarter of 2021. The concentration and elemental composition of $PM_{2.5}$, PM_{coarse} and PM_{10} pollution have been monitored systematically since 1997 at an urban background site (Borbély-Kiss et al., 1999; Dobos et al., 2009). We have thorough background knowledge about the composition and sources of PM pollution in the city. In the past decades, the main sources of PM pollution have been identified as biomass burning from domestic heating, traffic, secondary aerosols, mineral dust, sea salt, oil and coal combustion, waste incineration, construction, and biogenic emission (Almeida et al., 2020; Angyal et al., 2021; Furu et al., 2022; Kertész et al., 2010; Major et al., 2021).

The sampling location was the premises of ATOMKI in Debrecen, Hungary (47.54445, 21.62340) (Fig. 1). The site is situated in a residential area, 1.5 km from the city center. Close to the sampling location, there are two main traffic roads and two tram lines. The ATOMKI site can be classified as urban background (UB) since it is not significantly influenced by any single source but rather a combination of sources upwind of the station (EEA, n.d.-a).

During 2018 and 2019, intensive construction work was underway within a few hundred meters. In March 2021, the reconstruction of a nearby intersection started, along with the replacement of utilities on another main road in the close vicinity of the site. The roadwork continued until 2022.

In March and April 2020, major landscaping works were carried out to prepare the BMW factory site, which lies 10 km NW from the ATOMKI station. There are three fixed monitoring stations of the Hungarian Air Quality Monitoring Network (OLM) in the city of Debrecen (OMSZ, n.d.-b). In general, daily and hourly mean concentrations of air pollutants like O_3, CO, PM_{10}, NO, NO_2, SO_2, etc. are available at these stations. In this work, daily concentrations of NO_2, CO, NO_X, and PM_{10} were used as complementary data to our study because concentrations of these components were available at all stations without bigger gaps in the data series.

Meteorological data corresponding to Debrecen was available from the repository of the Hungarian Meteorological Service (OMSZ, n.d.-b), while planetary boundary layer heights (PBLH) were collected from the Copernicus Climate Data Store using ERA5 reanalysis dataset (Hersbach et al., 2020, 2023). PBLH data was collected with hourly resolution for a

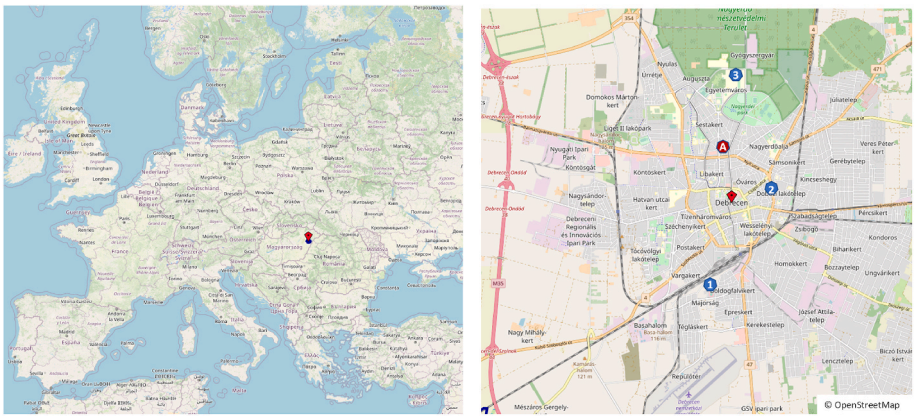

Fig. 1. Map of the investigated area. (A): UB sampling site at ATOMKI, (1) Kalotaszeg tér UB monitoring site of the Hungarian Air Quality Monitoring Network (HAQN), (2): Hajnal utca Traffic monitoring site of HAQN, (3): Klinika SUB monitoring site of HAQN.

0.25° x 0.25° grid cell which included Debrecen.

2.2. PM sampling

24h aerosol samples were collected by a Gent-type Stacked Filter Unit (Gent SFU) (Hopke et al., 1997) twice a week, on working days. $PM_{2.5}$ and PM_{coarse} (particles with aerodynamic diameter between 2.5 and 10 μm) fractions were sampled separately on nucleopore polycarbonate filters. Usually, the sampling started at 10:00 a.m., and the flow rate was set to 16–17 l/min. The sampling period was from March 2018 to March 2022.

2.3. Filter analysis

In order to obtain the PM mass concentration, the samples together with field blanks were weighed before and after sampling with a Radwag microbalance model MYA5 (resolution 1 μg). The filters were conditioned at relative humidity of ~50% and temperature of 22–24 °C for at least 24 h, and the weighing was done under these conditions. An antistatic ionizer was used to eliminate possible static electricity from the filters.

The elemental composition of the samples was determined by Particle Induced X-ray Emission (PIXE) analytical method (Maenhaut, 2015) at the in-air millibeam PIXE setup of the ATOMKI Tandetron accelerator (Rajta et al., 2018). For the irradiation, a proton beam of 2.5 MeV energy and of 50–60 nA was used. The accumulated charge on each sample was 10 μC. The PIXE measurements were carried out in He atmosphere; this way, elements with $Z > 6$ could be detected. The samples were scanned in front of the beam in order to avoid beam damage and to increase the area of analysis. A detector cluster consisting of three 65 mm^2 Be windowed SDD and one 30 mm^2 ultra-thin windowed (UTW) SDD X-ray detector recorded the characteristic X-ray lines emitted from the samples. 125 μm thick Kapton absorbers were used in front of the Be windowed detectors, while a pair of strong permanent magnets protected the UTW detector from the scattered protons. A detailed description of the setup, detection limits, and other analytical characteristics can be found in (Aljboor et al., 2023).

In order to increase the sensitivity of the method (and decrease the limit of detection), the spectra recorded by the three identical Be-windowed detectors were summed up. The obtained X-ray spectra were evaluated by the GUPIXWIN program code (Campbell et al., 2010). The concentration of 25 elements (O, Na, Mg, Al, Si, P, S, Cl, K, Ca, Ti, V, Cr, Mn, Fe, Co, Ni, Cu, Zn, As, Br, Rb, Sr, Zr, Ba, and Pb) was determined, after blank correction. The analytical uncertainty varied between 5 and 15%, depending on the element and its concentration (see Table S1 in Supplementary Materials).

The mineral dust component was calculated as follows (Cohen et al., 2020):

$$1.46[Mg] + 1.9[Al] + 2.14[Si] + 1.4[Ca] + 1.67[Ti] + 1.42[Fe] \quad (1)$$

A portable **M**ulti-Wavelength **A**bsorption **B**lack Carbon **I**nstrument (MABI) developed by ANSTO (Manohar et al., 2021) was applied to analyze the light-absorbing carbon (BC) content of the samples. For the BC analysis, the procedure described in (Manohar et al., 2021) was followed. BC concentrations presented in this work were determined at $\lambda = 639$ nm. The difference between concentrations determined at $\lambda = 405$ nm and $\lambda = 1050$ nm was used to distinguish between fossil fuel combustion and biomass burning.

2.4. Statistical analysis and model calculations

Spearman correlations were applied to study the relationship between the components of PM in the different time periods. Non-parametric Mann-Whitney U tests were employed to explore whether the differences were significant (with a significance level of 0.05) between the two data groups corresponding to the pre-COVID and COVID periods.

The relative change between the data means or medians measured during a lockdown and the corresponding baseline period was calculated according to the following formula:

$$RC\ (\%) = [\text{mean}\ (\text{Lockdown}_x) - \text{mean}\ (\text{Baseline}_x)]/\text{mean}\ (\text{Baseline}_x) * 100 \quad (2)$$

Source apportionment was performed applying the widely used Positive Matrix Factorization (PMF) method (Brown et al., 2015; Hopke, 2016; Paatero and Tapper, 1994). PMF model version 5.0 was applied separately for the fine and coarse fractions. Each data matrix contained 340 samples and over 20 variables. A detailed description of the PMF analysis is in the Supplementary Materials.

In order to identify the origin of specific pollutants and to distinguish between local, regional, and remote contributions, trajectory statistical methods (TSM) were employed (Di Gilio et al., 2015; Neykova and Hristova, 2020; Squizzato and Masiol, 2015).

In this work, 96-h backward trajectories starting at the sampling site were calculated using the NOAA HYSPLIT model version 5.2 (Stein et al., 2015). Archived meteorological data from the Global Data Assimilation System (GDAS1) were used. For each day, back-trajectories were computed at 12:00, 20:00 and 4:00 CET at different starting heights (200, 500 and 1000 m AGL) using the default vertical motion: model vertical velocity. In this work, trajectories with starting height of 1000 m were used which represents the height of the mixing layer in Debrecen.

Cluster analysis (CA) of the back trajectories, Potential Source Contribution Function (PSCF) and Concentration Weighted Trajectory

(CWT) calculations were performed using the HYSPLIT model and 'openair' R package (Carslaw and Ropkins, 2012), respectively.

Trajectory clustering gives information about the origin of air masses that arrive at the site. PSCF calculates the probability that a source is located at a coordinate (i,j) (at latitude *i* and longitude *j*), while CWT provides weighted concentration fields.

The 4-day backward trajectories served as the input variable for the cluster analysis. For each cluster, an average trajectory was calculated.

The PSCF is based on the assumption that if a source is located at a cell with coordinates *i* and *j*, the material from the source can be collected and transported along the trajectory to the receptor location with an air parcel passing through this location.

PSCF solves the following equation (3):

$$PSCF = \frac{m_{ij}}{n_{ij}} \tag{3}$$

where n_{ij} is the number of occasions when a trajectory passes the cell with coordinates (i,j), and m_{ij} is the number of occasions associated with high pollution levels at the receptor site. The resulted value can be explained as the probability that concentrations larger than a threshold value are related to the passage of air parcels through the grid cell (i,j). Therefore, this method is suitable for identifying the possible geographic origin of a pollutant. In this study, we used the 75th percentile as the threshold criterion.

In CWT, a weighted mean concentration of the given pollutant is calculated for each grid cell of the domain according to equation (4). The weighing factor is the cumulative residence time of all the associated trajectories in the grid cell.

$$C_{ij} = \frac{1}{\sum_{l=1}^{M} \tau_{ijl}} \sum_{l=1}^{M} C_l \tau_{ijl} \tag{4}$$

where C_{ij} is the average weighted concentration in the grid cell (*i,j*), *l* is the trajectory index, *M* is the number of trajectories associated with the grid cell (*i,j*), τ_{ijl} is the residence time of trajectory l at the cell (*i,j*), and C_l is the concentration measured at the receptor site associated with trajectory *l*. Consequently, areas with high CWT values in the concentration field mean that air parcels residing over them resulted in elevated pollution levels at the receptor site, i.e. these are the potential source areas of the air pollutant in question.

2.5. The studied period

This study covers the period from March 2018 to March 2022. The first 2 years serve as the baseline to which the corresponding periods of the next two years are compared.

The period affected by COVID-19 in Hungary lasted from early 2020 to March 2022. During this time, there were 4 lockdowns and 2 relaxation periods, as listed in Table 1 and shown in Fig. 2. The four lockdowns were related to the 4 waves of COVID. The two years of the pandemic have been broken down into 10 periods: the four lockdowns that coincided with springs (LD1 and 3) and winters (LD2 and 4), the summers of the relaxation periods, the first two months of autumn, which belonged to the relaxation, and the Novembers, which were transition time into lockdowns and also to winters (named par(tial)-lockdown in 2020 and pre-lockdown in 2021). The reason why September–October was handled separately was the different activity of the population: this is the time when work and school start after summer vacation. November is the beginning of the heating season, and during this month high pollution level episodes occur frequently due to elevated emission of pollutants and unfavorable meteorological conditions, e.g., temperature inversions.

We used the stringency index introduced by the OxCGRT project (Hale et al., 2021) to characterize a lockdown period. It is a complex measure of nine factors, such as school and workplace closures, cancellation of public events, restrictions on public gatherings, stay-at-home requirements, restrictions on internal movements and international travel, etc. Data were obtained from the Our World in Data online resource (Mathieu & et al., n.d.). The stringency index in the first 3 lockdown periods was very similar; however, there were differences in the measures.

The first lockdown was the most severe: Hungary closed its borders (only transits were allowed), all public and sporting events were cancelled and banned, entertainment venues and cinemas were closed, universities, schools, nurseries, and kindergartens were closed, there were production shutdowns in factories, and most of the population switched to home office. There was a general curfew except for work and subsidiary purposes. The use of public transportation was not suggested, and at the same time, parking was free. Free parking stayed until the end of the pandemic. During the second lockdown, some of the restrictions were relaxed: children under 14 could attend primary schools, kindergartens and nurseries, and individual outdoor sport activity was allowed. Curfew was in force from 8 p.m. to 5 a.m. Then, in the third lockdown all schools, kindergartens and nurseries were closed again. Home office was optional and recommended. In the 4th lockdown, when the majority of the population was already vaccinated, the measures corresponded mainly to mandatory mask wearing in closed places. Only unvaccinated people were subject to more strict measures.

The change in mobility gives a good description of the change in people's lifestyle due to closures and restrictions (Borkowski et al., 2021; Bucsky, 2020). For the region (Hajdú-Bihar county), Google mobility data was available (Google, n.d.). Although it corresponds only to people with mobiles, we are probably not far from the truth if we consider these data to be representative of a city that is a cultural and academic center. During lockdowns, the mobility of the population in residential areas increased by about 10%, while in recreation areas, transit stations and workplaces, it decreased by 20–40%. The biggest change was during the first lockdown, and the smallest during the last. In the relaxation periods, mobility was close to the levels of the baseline, whereas increased activity could be observed in parks, retail and recreational facilities, especially in the 2nd year of the pandemic.

Besides the characteristics of the lockdown and relaxation periods, meteorological parameters affecting air pollution are also listed in Table 1. Considering the whole 2-year-long period of the pandemic, the meteorological parameters were very similar to the previous two years. The differences over the investigated seasons and other periods will be discussed together with the results.

3. Results and discussion

3.1. The evolution of air pollutants in Debrecen

Average concentrations of CO, NO_2, NO_x and PM_{10} measured at the three AQ monitoring stations in Debrecen, as well as the averages of PM_{10}, $PM_{2.5}$ and PM_{coarse} at ATOMKI are presented in Table 2 for the 2-year-long (pre- and COVID) periods and broken down to the above-described lockdowns and relaxation periods, too. Fig. 3 shows the relative change of averages to the corresponding baseline data.

The highest concentrations of all pollutants were measured at the traffic site. Compared to the background stations, the biggest difference was observed for NO_x; its concentration was 50–60% less at the background sites than at the traffic site. In the case of NO_2, the difference in average concentrations was around 40%, while for CO and PM_{10} it was less than 10%. During the time of the pandemic, this difference between the traffic site and background sites decreased, indicating a decrease of traffic emission and a shift in mobility into residential areas. All pollutants showed a seasonal pattern: the highest concentrations were measured in the heating season (November–April), showing that domestic heating is another major source of air pollution in Debrecen. NO_x/CO ratios can give a rough estimate about the relative contribution of traffic and biomass burning at a site, since this ratio differs significantly for the two emission types: the traffic emission ratio is much

Table 1
Stringency index, meteorological parameters and change in mobility during the 10 investigated periods of the COVID-19 pandemic (2020–2022) and the corresponding baseline values (pre-COVID) from years 2018-19.

Time period	date		Stringen-cy index	METEOROLOGY								MOBILITY					
				precip.	temp	air pressure	rel. humidity	wind speed	WS < 1 m/s	PBLH	PBLH <50 m	change in % compared to baseline (2018–2019)					
	start	end		month avg. (mm)	daily avg. (°C)	daily avg. (hPa)	daily avg. (%)	daily avg. (m/s)	days month avg	daily avg. (m)	hours month avg	retail, recreat.	grocery, pharm.	resi-dential	transit stations	parks	work-places
COVID	**2020–03–01**	**2022–02–28**		**37.3**	**11.4**	**1003.9**	**73.4**	**3**		**682**		**−8.9**	**5.9**	**5.7**	**−17.4**	**43.0**	**−19.8**
lockdown1	2020-03-11	2020-05-31	71.8	28.2	10.9	1004.3	57.7	3.7	1	784		−38.0	−15.0	13.2	−40.9	1.8	−34.0
relax1 - summer	2020-06-01	2020-08-31	54.6	82.8	21.5	1000.3	71.8	2.8	1	997		0.6	0.0	2.7	−15.6	86.5	−21.7
relax1 - autumn	2020-09-01	2020-10-31	42.3	56.1	15.2	1003.0	77.5	2.8	2	805		−4.7	1.2	2.1	−10.7	45.0	−15.0
par-lockdown2	2020-11-01	2020-11-30	66.2	15.6	5.0	1014.4	92.4	1.8	7	468	126	−23.8	−2.7	8.0	−26.0	1.4	−20.8
lockdown2	2020-12-01	2021-03-08	72.4	40.7	2.6	1003.3	87.6	2.9	7	376	104	−33.5	−4.1	10.2	−33.6	−3.2	−25.7
lockdown3	2021-03-08	2021-05-17	72.6	35.0	9.5	1003.4	66.7	3.5	1	756		−20.8	2.9	7.8	−23.9	33.3	−22.0
relax2 - summer	2021-06-01	2021-08-31	33.9	25.7	22.8	1001.4	62.1	2.9	0	973		15.8	22.3	0.3	−0.2	120.7	−15.5
relax2 - autumn	2021-09-01	2021-10-31	28.3	14.7	13.2	1007.8	69.6	2.5	3	698		16.4	23.4	0.5	5.4	72.6	−9.2
pre-lockdown 4	2021-11-01	2021-12-10	29.9	41.5	5.3	1004.7	88.1	2.3	3	398	172	6.1	21.3	4.2	−5.9	26.1	−11.8
par-lockdown4	2021-12-11	2022-03-06	49.4	19.6	1.4	1005.0	83.4	3.5	4	347	140	1.2	17.2	6.2	−12.7	18.1	−13.9
pre-COVID	**2018–03–01**	**2020–02–28**		**35.3**	**12.4**	**1003.6**	**73.3**	**3**		**726**							
2018, 2019	1-Mar	31-May		43.4	12.5	1000.8	66.8	3.5	1	767							
2018, 2019	1-Jun	31-Aug		36.9	22.6	1001.6	67.1	2.8	0	1010							
2018, 2019	1-Sep	31-Oct		19.3	15.3	1006.1	67.8	2.5	5	853							
2018, 2019	1-Nov	30-Nov		55.7	8.2	1004.5	84.5	2.7	1.5	488	70						
2018–2020	1-Dec	28-Feb		29.0	1.4	1006.5	85.9	3.1	6	399	85						

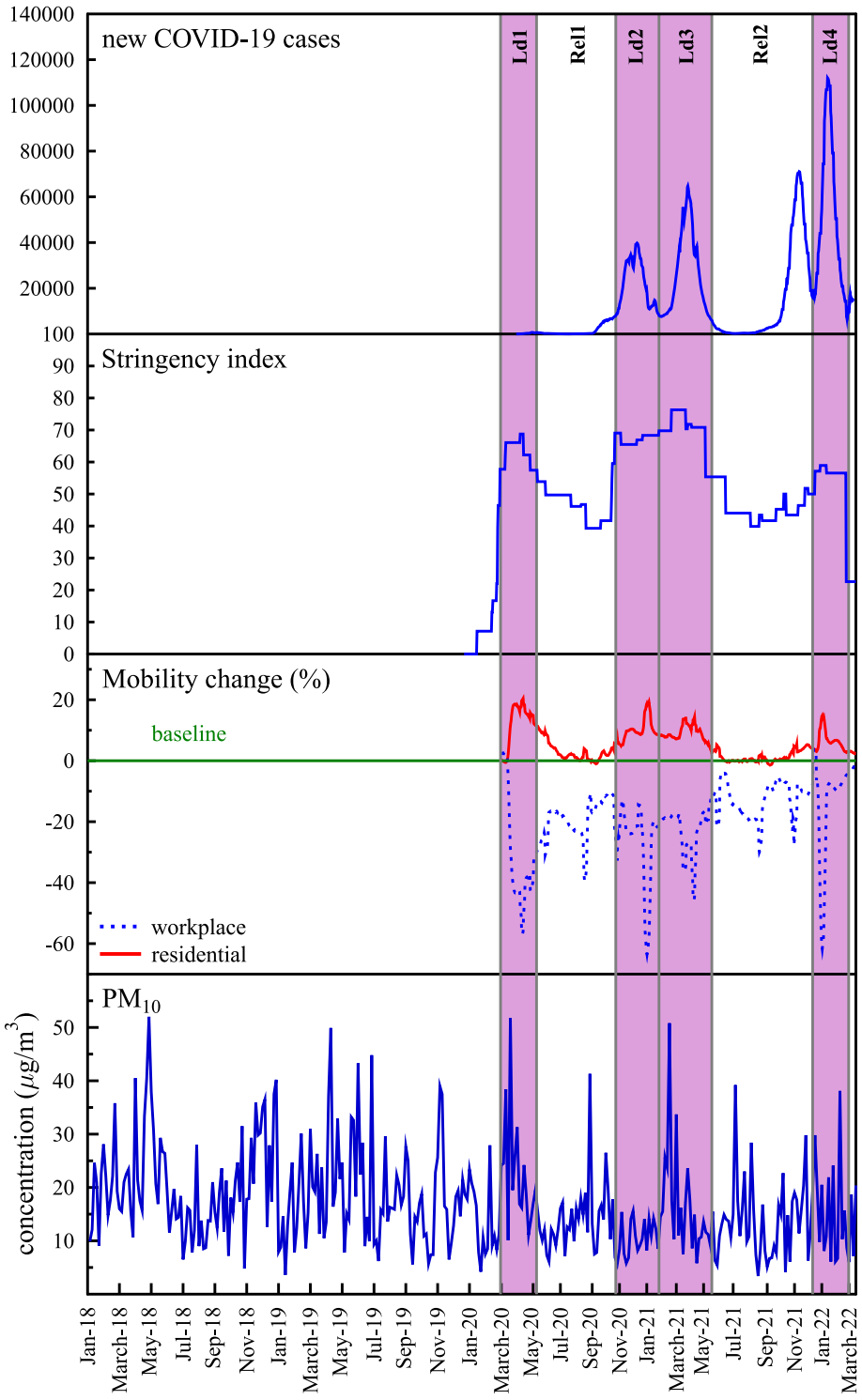

Fig. 2. New COVID cases, stringency index, mobility change and PM_{10} concentrations at ATOMKI from March 2018 to February 2022. The lockdown (Ld1-4) and relaxation periods (Rel1-2) are indicated on the figure.

larger than the one of biomass burning (Kalogridis et al., 2018).

In general, the concentration of the pollutants decreased by ~20% during the 2 years of the pandemic at all sites. The exception is CO, whose concentration remained or even increased at the Klinika site. This suburban monitoring site can be found on the premises of the clinic campus, which is part of the county hospital. For obvious reasons, this site was even busier during the pandemic than before; therefore, we did not expect a significant decrease in air pollutants here. Indeed, here the concentration of traffic-related gaseous pollutants increased with the increasing number of new COVID cases, as can be seen in Fig. 3.

The largest decreases in pollutants were observed during lockdowns (20–30% on average). In the relaxation periods, concentrations remained below the baseline by 10–20%. The change in the NO_x/CO ratios showed a significant increase in the relative contribution of biomass burning at the expense of traffic emissions during the lockdowns which all fell on the heating period.

In the case of all pollutants and all sites, the yearly average concentrations were well below the limit values set by the EU in Directive

Table 2
Average concentrations in mg/m^3 of NO_2, CO, NO_x, PM_{10} and NO_x/CO ratios at the 3 AQ monitoring sites in Debrecen during the 10 investigated periods during the COVID-19 pandemic and the corresponding baseline values (pre-COVID) from years 2018-19. The last columns contain PM concentrations (in μg/m^3) and $PM_{2.5}/PM_{10}$ ratios measured at the urban background site in ATOMKI.

	Hajnal utca - TRAFFIC					Kalotaszeg tér - UB					Klinika - SUB					ATOMKI - UB			
	NO_2	CO	NO_X	NO_x/CO	PM_{10}	NO_2	CO	NO_X	NO_x/CO	PM_{10}	NO_2	CO	NO_X	NO_x/CO	PM_{10}	PM_{coarse}	$PM_{2.5}$	PM_{10}	$PM_{2.5}/PM_{10}$
COVID	26.7	531	57.8	0.109	22.2	16.4	473	27.7	0.059	20.6	23.7	451	28.9	0.064	19.1	6.7	8.2	14.9	0.55
lockdown1	25.9		53.4		23.8	16.9	406	24.7	0.061	25.6	21.8		25.6		21.7	12.3	8.8	21.1	0.42
relax1 - summer	22.7	397	40.2	0.101	18.8	11.5	310	15.4	0.050	16.3	17.2	283	19.9	0.070	16.8	6.1	7.7	13.9	0.55
relax1 - autumn	30.5	480	72.3	0.151	25.7	17.6	444	29.6	0.067	19.3	26.9	482	34.4	0.071	19.6	6.9	5.9	12.8	0.46
par-lockdown2	28.1	527	69.3	0.132	23.9	19.6	521	32.7	0.063	21.1	25.7	531	31.5	0.059	21.5	3.2	7.5	10.6	0.71
lockdown2	28.2	597	64.6	0.108	23.3	20.2	587	32.5	0.055	22.1	27.0	553	32.5	0.059	22.8	4.9	11.2	16.1	0.70
lockdown3	24.4	561	46.4	0.083	17.3	13.3	465	18.2	0.039	16.1	20.5	327	24.0	0.073	16.1	5.9	7.0	12.9	0.54
relax2 - summer	23.0	435	37.7	0.087	18.7	10.6	229	18.2	0.079	20.9	19.7	309	21.9	0.071	18.1	6.7	7.0	13.7	0.51
relax2 - autumn	32.4	566	78.8	0.139	24.8	23.4	596	48.7	0.082	24.2	32.2	466	40.6	0.087	21.3	7.1	8.0	15.2	0.53
pre-lockdown 4	30.5	635	93.5	0.147	33.8	23.7	761	57.1	0.075	27.5	37.0	726	55.8	0.077	21.9	5.2	11.6	16.8	0.69
lockdown4	29.0	668	69.6	0.104	23.2	17.5	679	31.8	0.047	18.9		608			15.5	4.0	9.5	13.5	0.70
pre-COVID	**37.3**	**545**	**71.9**	0.132	**27.3**	**20.7**	**445**	**31.9**	**0.072**	**25.3**	**24.0**	**384**	**30.2**	**0.079**	**24.1**	**8.3**	**10.9**	**19.2**	**0.57**
March-May	36.6	482	60.1	0.125	25.1	19.2	330	26.4	0.080	23.7	16.2	295	19.4	0.066	21.9	12.0	10.5	22.5	0.47
June-Aug	33.7	439	43.5	0.099	21.3	14.4	331	18.6	0.056	19.9	14.3	338	17.1	0.051	19.4	7.9	8.9	16.9	0.53
Sep-Oct	45.3	591	90.6	0.153	32.2	23.8	451	37.1	0.082	27.0	34.3	468	42.9	0.092	24.9	10.6	10.0	20.5	0.49
Nov	38.4	656	91.7	0.140	31.8	25.4	554	46.0	0.083	31.6	28.0	486	36.9	0.076	24.5	5.0	9.8	14.8	0.66
Dec-Feb	37.5	680	87.6	0.129	29.5	23.7	589	39.9	0.068	28.9	31.2	446	41.5	0.093	27.2	5.6	12.4	18.0	0.69

(2008)/50/EC (40 μg/m^3 for PM_{10} and NO_2, 70 μg/m^3 for NO_x and 3000 μg/m^3 for CO) (EEA, n.d.). Exceedances of daily (24h) limit values happened only in the case of PM_{10}. In the 2 years before the pandemic, there were 49, 48 and 29 at the traffic, UB and SUB sites, respectively. During the 2 years of COVID, these values were 23, 24 and 7, so a drop of at least 50% was achieved here. 90% of exceedances occurred in November and in the winter months.

At the ATOMKI urban background (UB) site, usually lower PM_{10} concentrations are measured; however, PM_{10} data from all stations correlates strongly with each other. The difference originates from the different methods, i.e., standard gravimetry of filter samples vs automatic station data. A detailed explanation of this phenomenon can be found in (Angyal et al., 2021).

For both PM_{10} and $PM_{2.5}$, the yearly average was well below the EU limit values (40 and 25 μg/m^3, respectively). In the case of $PM_{2.5}$, the WHO Air Quality Guideline (AQG) value for the yearly average is 5 μg/m^3, and 15 μg/m^3 is the recommended 24-h limit value (World Health Organization, 2021). $PM_{2.5}$ concentrations exceeded this limit several times. The exceedances occurred mainly in the heating periods. The proportion of polluted days (i.e., when the concentration was higher than 15 μg/m^3) to sampling days also decreased significantly during the COVID compared to the baseline. E.g., in winter, the $PM_{2.5}$ concentrations exceeded the WHO AQG value in almost 50% of the sampling days, while during the years of COVID, this value was reduced to under 20%. The $PM_{2.5}/PM_{10}$ ratio was 0.57±0.15 for the whole period, changing from 0.7 in the heating season to 0.5 on average for the summer, which is consistent with our earlier observations (Furu et al., 2022; Kertész et al., 2010). There was no significant change in the $PM_{2.5}/PM_{10}$ ratio.

The behavior of air pollutants differed from what was expected during lockdown1 and lockdown4. Despite the strict measures and the fact that life in the city had virtually come to a standstill, the expected drastic reduction of pollution failed to materialize during the first lockdown. The exact opposite happened during lockdown4: while there were basically no restrictions and life was back to almost normal, the concentrations of most pollutants were 25–30% less than those of the baseline. The study of composition, sources, meteorological conditions, and geographical source areas might provide answers to these questions.

3.2. *Elemental composition of PM_{coarse} and $PM_{2.5}$*

The average concentrations of PM and the measured species for the two time periods are summed up in Tables 3 and 4 for the coarse and fine fractions, respectively. The time series of PM_{coarse} and $PM_{2.5}$ and their major components are presented in Figs. S1–S6 in Supplementary Materials.

Presuming that S appears as SO_4^{2-} (Yao et al., 2003) and mineral dust elements are present in their common oxide form, the measured components account for 40–50% of the total PM mass. It can be assumed that organic carbon (OC), nitrate (NO_3^-) ammonia (NH_4^+) and water make up the unmeasured part of PM mass.

The major components of PM_{coarse} were mineral dust, with over 30% contribution in both time periods. For $PM_{2.5}$, BC (14–16%), SO_4^{2-} (17–20%) and mineral dust (11.5–14%) were the main constituents. These results are in agreement with our previous findings (Angyal et al., 2021; Furu et al., 2022; Kertész et al., 2010) and data from other studies corresponding to urban sites in the region (Almeida et al., 2020; Rys et al., 2022).

The time series of both PM size fractions and their components show strong seasonality. In the case of $PM_{2.5}$ as well as BC, K, Pb and Zn, winter maximums and summer minimums can be seen. These components are strongly related to domestic heating, which explains their enhanced presence in the heating period. In the case of the fine fraction S, there was no difference between the seasons, while the coarse fraction S had winter maxima, indicating that its source was most probably local heating (see Fig. S6). The origin of S in $PM_{2.5}$ is regional transport, which will be discussed later. Mineral dust elements in both size fractions show

		March 2020- Feb. 2022	lockdown1	relax1 - summer	relax1 - autumn	par-lockdown2	lockdown2	lockdown3	relax2 - summer	relax2 -autumn	pre-lockdown4	lockdown4
Hajnal utca (Traffic)	NO_2	-28	-29	-33	-33	-27	-25	-33	-32	-29	-21	-23
	CO	-3		-10	-19	-20	-12	17	-1	-4	-3	-2
	NO_X	-20	-11	-8	-20	-25	-26	-23	-13	-13	2	-21
	PM10	-19	-5	-12	-20	-25	-21	-31	-13	-23	6	-21
	NO_x/CO	-18		2	-2	-6	-16	-34	-13	-9	5.5	-19
Kalotaszeg tér (UB)	NO_2	-21	-12	-20	-26	-23	-15	-31	-26	-1	-7	-26
	CO	6	23	-6	-1	-6	0	41	-31	32	37	15
	NO_X	-13	-6	-17	-20	-29	-19	-31	-2	31	24	-20
	PM10	-19	8	-18	-29	-33	-24	-32	5	-10	-13	-35
	NO_x/CO	-18	-24	-12	-19	-24	-18	-51	41	-1	-10	-31
Klinika (SUB)	NO_2	-1	35	21	-22	-8	-13	27	38	-6	32	
	CO	17		-16	3	9	24	11	-9	-1	49	36
	NO_X	-4	32	17	-20	-15	-22	23	28	-5	51	
	PM10	-21	-1	-14	-21	-12	-16	-27	-7	-14	-11	-43
	NO_x/CO	-19		39	-22	-22	-37	12	40	-5	1	
ATOMKI (UB)	PM_c	-20	3	-23	-35	-36	-13	-51	-15	-33	4	-29
	$PM_{2.5}$	-25	-16	-13	-41	-23	-10	-33	-21	-20	18	-23
	PM_{10}	-22	-6	-18	-38	-28	-11	-43	-19	-26	14	-25
	$PM_{2.5}/PM_{10}$	-3	-11	5	-5	7	1	16	-3	8	4	2

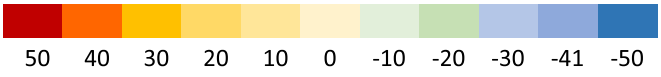

Fig. 3. Relative change (%) in concentrations of pollutants at 4 monitoring sites in Debrecen.

maximums in springs and autumns and minimums in winter. The same tendency can be observed for PM_{coarse}. The explanation of this trend must be sought in meteorology and seasonal agricultural work. Phosphorus, which is a fingerprint element of biogenic emission, is present in high concentrations during the vegetation period. Elements related to traffic (e.g., Cu) did not show seasonal trends.

Several episodes can be seen in the time series of mineral dust; these are related to Saharan and Asian dust episodes and local dust events. Backward trajectories together with maps of dust optical depth by MONARCH model of the WMO Barcelona Dust Regional Centre (Pérez et al., 2011) and the composition of the given sample help to distinguish between these episodes. E.g., local sandstorms can be characterized by a relatively high Si content, while Saharan dust usually contains a high amount of Ti and Fe. There were several Saharan episodes in all investigated years, typically in spring (see Figs. S7a and S7b). Aerosols collected on March 26, 2020 contained Mg and Sr in unusually high concentrations. Backward trajectories revealed that they originated from Asia, the region of the Caspian Sea, and the Karakum Desert (Fig. S8).

The case of chlorine is never simple: it can have many different sources in both size fractions, such as salt, buildings, pesticides, fertilizers, biomass burning, or industry (Angyal et al., 2010). In most cases, Cl in the coarse mode occurs in the form of salts, mainly NaCl; therefore we expect a strong correlation between Na and Cl. However, in Figs. S3a and S3b, Cl shows no correlation with Na in 2018, while from 2019 they move together. By calculating pairwise correlations for these two periods, it turned out that the correlation coefficient (r) between Cl and Na was 0.6 for 2018, while from 2019 it was the expected 0.9. In the meantime, the Cl:Ca correlation was 0.6 for 2018 and there was no correlation between these two elements from 2019. Ca together with Cl originates from constructions (Angyal et al., 2010). Indeed, in 2018 the foundation works for a tower block were carried out nearby. In the fine fraction, Cl concentrations above detection limit were measured only during the heating period; therefore, fine fraction Cl was attributed to biomass burning. The episodic peaks, especially in the winter of 2021-22, appeared together with Na; therefore, its source was most probably sea salt, which assumption was confirmed by backward trajectory calculations, too (Fig. S9).

Black carbon (BC) was one of the main components of $PM_{2.5}$; its concentration varied between 0.7 $\mu g/m^3$ (summer) and 2 $\mu g/m^3$ (heating season), and the average seasonal contribution ranged between 7% (summer) and 17% (winter). In an urban environment, its main source is vehicular traffic and biomass burning (BB) (Rajesh and Ramachandran, 2017; Salma et al., 2020a). The correlation to tracer elements like K and

Table 3
Average (AVG), median (MED), standard deviation (SD), minimum (Min), and maximum (Max) concentrations of PM_{coarse}, and its components (in ng/m^3) and contribution of some components to the PM mass in % for the pre-COVID (March 2018–Feb. 2020) and the COVID period (March 2020–Feb. 2022).

	Pre- COVID (ng/m^3)					COVID (ng/m^3)				
	AVG	MED	SD	Min	Max	AVG	MED	SD	Min	Max
PM_{coarse}*	8300	6100	6300	700	36600	6700	4600	5500	1000	27500
Na*	83	67	63	< DL	322	81.5	39	175	< DL	1461
Mg*	45.5	32	42	< DL	316	34.5	25	38	< DL	327
Al*	230	146	240	12	1705	166	120	160	2.0	812
Si*	781	527	790	38	6007	591	445	539	6.6	2631
P*	11	9.4	8.3	1.8	43	8.4	7.5	5.7	1.6	27
S*	93	72	68	18	398	73	45	106	5.2	1166
Cl*	104	68	108	3.8	638	58	19	19	1.9	1868
K*	109	80	87	22	593	92	70	74	11	369
Ca*	263	199	222	16	1499	226	175	213	15	1752
Ti*	16	11	16	0.2	127	12.3	9.2	12.8	< DL	60
V	0.6	0.4	0.6	< DL	4.0	0.9	0.4	1.2	< DL	6.3
Cr	0.6	< DL	1.0	< DL	9.3	0.4	0.1	0.7	< DL	3.5
Mn	6.9	5.6	5.1	0.9	38	6.8	5.8	4.9	0.3	26.1
Fe*	238	182	188	44	1202	189	148	156	28	882
Co*	1.8	1.5	1.1	0.3	7.1	1.6	1.3	1.3	< DL	7.0
Ni	0.5	0.4	0.3	< DL	1.8	0.4	0.2	0.4	< DL	1.8
Cu*	2.0	1.5	1.7	< DL	9.2	1.3	1.0	1.3	< DL	7.6
Zn*	4.6	3.7	3.2	0.6	15	3.6	2.7	2.9	0.7	19
Br	0.3	0.2	0.3	< DL	1.6	0.4	0.2	0.4	< DL	2.3
Ba*	6.0	5.0	3.3	< DL	19	4.9	4.3	3.1	1.1	17
Pb	2.2	1.7	1.5	< DL	6.7	2.0	1.4	1.9	< DL	12
Min. dust*	2915	2016	2747	198	18710	2242	1726	1991	86	9837
SO_4*	280	217	204	55	1193	218	136	318	16	3499
PM10*	19200	17400	9500	3600	52000	14900	8300	13800	3400	51800
Contributions of components (%)										
Min. dust	32.4	33.4	10	3.1	52.4	31.0	31.0	11.5	3.9	65.4
SO_4	4.7	3.2	4.5	0.9	36	3.8	2.6	3.4	0.4	18

*indicates species where the change was significant according to the Mann-Whitney *U* test.

Table 4
Average (AVG), median (MED), standard deviation (SD), minimum (Min), and maximum (Max) concentrations of $PM_{2.5}$, and its components (in ng/m^3) and contribution of some components to the PM mass in % for the pre-COVID (March 2018–Feb. 2020) and the COVID period (March 2020–Feb. 2022).

	Pre-Covid ng/m^3					Covid ng/m^3				
	AVG	MED	SD	Min	Max	AVG	MED	SD	Min	Max
PM2.5*	10900	10100	5600	2200	32500	8200	7100	5200	1900	37300
BC	1520	1182	1116	97	5946	1280	926	1013	125	4778
Na*	61	50	42	3.2	213	72	43	155	2.8	1578
Mg	22	14.5	27.5	2.3	232	23	15	40	0.5	438
Al	102	61	121	1.9	974	87	55	109	< DL	934
Si	301	187	332	16	2326	268	183	294	15.1	2340
P	4.3	3.9	2.5	< DL	13.6	4.0	3.2	2.7	< DL	18
S	590	511	359	50	1770	498	404	272	80	1645
Cl*	5.3	3.1	5.3	1.1	33.3	12.1	4.8	34.0	< DL	302
K	194	146	145	20	773	169	115	165	22	1079
Ca	87	61	84	3	650	97	67	159	6.3	1799
Ti	6.1	3.7	7.2	< DL	52	5.4	3.4	7.1	< DL	61
V	0.4	0.4	0.3	< DL	1.7	0.6	0.4	0.7	< DL	4.1
Cr	0.6	0.4	0.6	< DL	2.7	0.2	DL	0.2	< DL	1.5
Mn*	4.6	3.7	3.9	0.4	25	6.2	5.7	3.2	0.8	20
Fe*	119	91	84	7.4	565	112	95	83	21.8	649
Co	1.0	0.9	0.6	< DL	3.7	1.1	0.9	0.8	< DL	6.6
Ni	0.4	0.4	0.3	< DL	1.5	0.3	0.2	0.3	< DL	2.7
Cu*	2.3	1.7	1.8	< DL	9.1	1.9	1.5	1.4	< DL	9.7
Zn*	11.4	9.2	7.9	1.7	49	9.3	6.7	7.4	1.4	41
Br*	1.0	0.8	0.7	< DL	3.5	1.5	1.1	1.4	< DL	8.5
Ba	2.8	2.3	2.0	< DL	11.2	3.0	2.6	2.4	< DL	21.4
Pb	5.0	4.1	3.7	< DL	23.5	4.4	3.4	3.5	< DL	18.4
Min. dust	1174	771	1206	73	9005	1079	760	1180	91	9177
SO_4	1771	1532	1078	149	5309	1493	1211	815	239	4936
Contributions of components (%)										
Min. dust	11.5	9.3	9.4	0.8	53.2	13.8	12.8	9.2	0.8	46.6
SO_4	16.6	15.6	6.3	4.1	34.7	20.0	19.5	7.0	2.8	42.3
BC	13.9	13.0	7.4	1.0	37.9	15.8	15.7	6.2	2.7	30.7

*indicates species where the change was significant according to the Mann-Whitney *U* test.

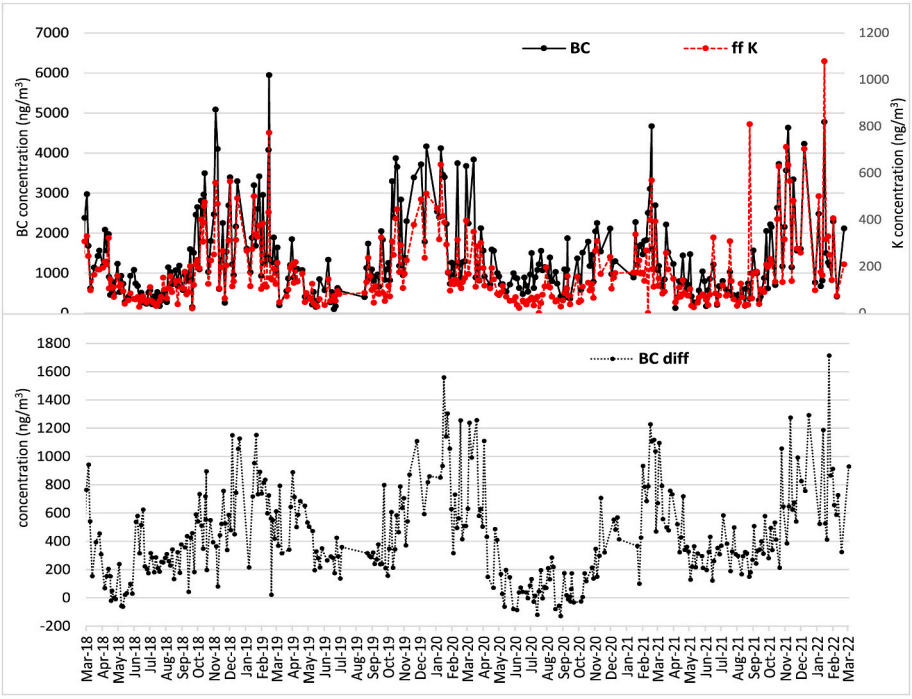

Fig. 4. Time trend of BC and K in $PM_{2.5}$ and concentration difference of BC measured at 405 and 1050 nm. (BC_{diff} = BC_{405nm}-BC_{1050nm}).

levoglucosan (Urban et al., 2012), as well as BC measurement at different wavelengths (Manohar et al., 2021; Mousavi et al., 2019) helps to distinguish between the sources. Fig. 4 shows the time trend of BC together with K and the concentration difference measured at 405 nm and 1050 nm. BC particles formed in high temperature diesel burning and lower temperature wood burning absorb at different wavelengths. The absorbance of BC due to BB is larger at shorter wavelengths, whereas it is higher at longer wavelengths for BC created in fossil fuel combustion. Therefore, the difference in concentrations determined at short (405 nm) and long (1050 nm) wavelengths can be used to separate these sources. When the concentration difference has a high positive value, BC originates from BB, and when it is around 0 or has negative values, the origin of BC is high-temperature fossil oil combustion.

Mann-Whitney *U* test showed no significant change in the BC concentration. The exception was summers, the relaxation periods, when the increase of BC concentration to the baseline was significant.

In the concentration of BC, there is a strong seasonal dependence. It has maximums in winter and minimums in summer. The fine fraction K correlates strongly to BC (r = 0.9) indicating that its main source is biomass burning. In winter, it is domestic heating via wood burning. From the concentration difference, it is also clear that in the heating season (November–March) its main source was BB, while in the summers it has traffic origin. However, Fig. 4 reveals additional interesting things. In 2018 and 2019, there were strong BB signals in September–October, whose origin is most probably field fires or burning of organic waste in gardens (it is a common practice even though it is prohibited by EU regulations) (Major et al., 2021). These indications disappeared completely during the COVID era, showing reduced activities in these areas, too. The BB peak in June 2018 could be traced back to forest fires in East-Ukraine (Fig. S10 in Supplementary Materials).

3.3. Sources of PM pollution in Debrecen

Source apportionment by positive matrix factorization resulted in 8 factors, both for the coarse and fine fractions. Figs. S11 and S12 (in Supplementary Materials) shows the factor profiles obtained for PM_{coarse} and $PM_{2.5}$, respectively. The following sources were apportioned to the factors of the coarse fraction: traffic, 2 types of soil, 2 types of combustion, roadworks, a mixed source of construction and Cl salts, and biogenic emission. In $PM_{2.5}$ traffic, soil types, biomass burning, combustion, roadworks, sea salt and secondary sulfates were identified as pollution sources.

Source contributions for the coarse and fine fractions are shown in Figs. 5 and 6, respectively. The factors apportioned to soil contain mineral dust elements like Mg, Al, Ca, Si, Ti, Fe, Rb, Sr and Ba. The presence of two soil factors is explained by the fact that the city lies on the borderline of a loess and a sandy area, as explained in paragraph 2.1. The contribution of soil to PM_{coarse} was about 50%, while to $PM_{2.5}$ it was 18%. The contribution of the soil factors was highest in spring and early autumn, while in winter it was almost negligible. The dry and windy weather favors the resuspension of dust, which is amplified by agricultural fieldwork. In addition, relatively frequent Saharan dust episodes, which typically occur in the spring, contribute significantly to the soil factors, too.

The traffic source is characterized by BC and heavy metals, like Cu, Fe, Co, Br, and Pb. These elements are tracers of vehicle transport, e.g., break, wear, tramway abrasion, and diesel fuel exhaust (Hudda et al., 2020; Kar et al., 2010). The contribution of traffic was 6% and ~12% for the coarse and fine fractions, respectively. Before the pandemic, the traffic source was the strongest in the months of the school year. During the years of COVID, this difference between the academic year and vacation time was equalized.

Biomass burning is one of the most important sources of $PM_{2.5}$. It is characterized by high K and BC concentrations. Its contribution was more than 50% during the heating season, while in the summer months it was not detectable. The factor identified as combustion is characterized by Zn, Pb, and Br to some extent. It is assumed that this originates from the boiler house of a nearby condominium or a secondary school dormitory next to the sampling site, which provides heating and warm water throughout the year. It has maximums in the heating season, like the BB source. A similar combustion source was found in the PM_{coarse}, too, with a 3% average contribution. Another factor of the coarse fraction characterized by high S content was apportioned to fossil fuel combustion from domestic heating. It had a yearly average contribution of 6%, with a maximum in winter and a minimum in summer.

The other dominant source of $PM_{2.5}$ is the factor 'secondary aerosol'.

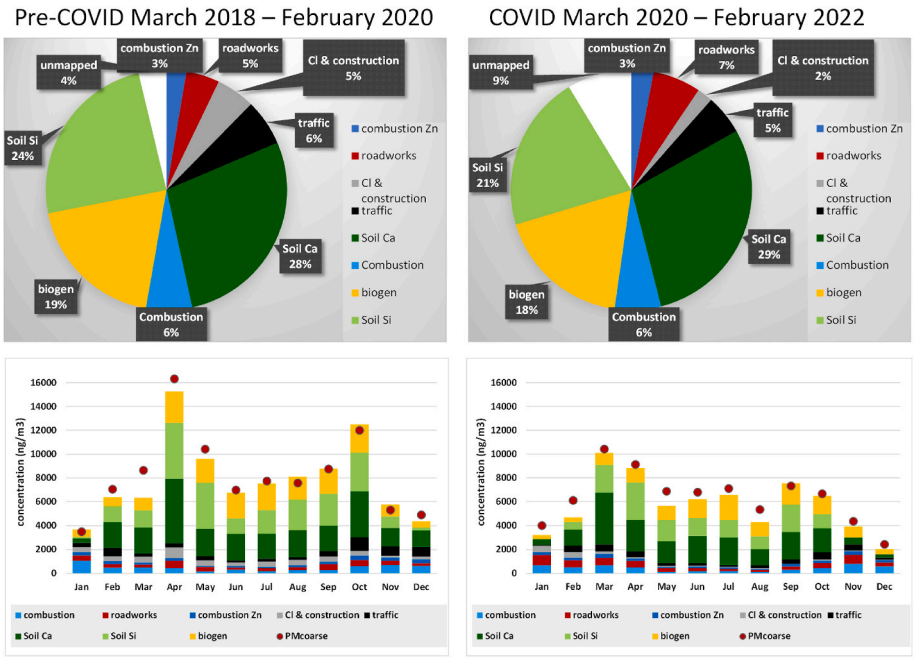

Fig. 5. Source contributions of PM_{coarse} before and during COVID-19 pandemic.

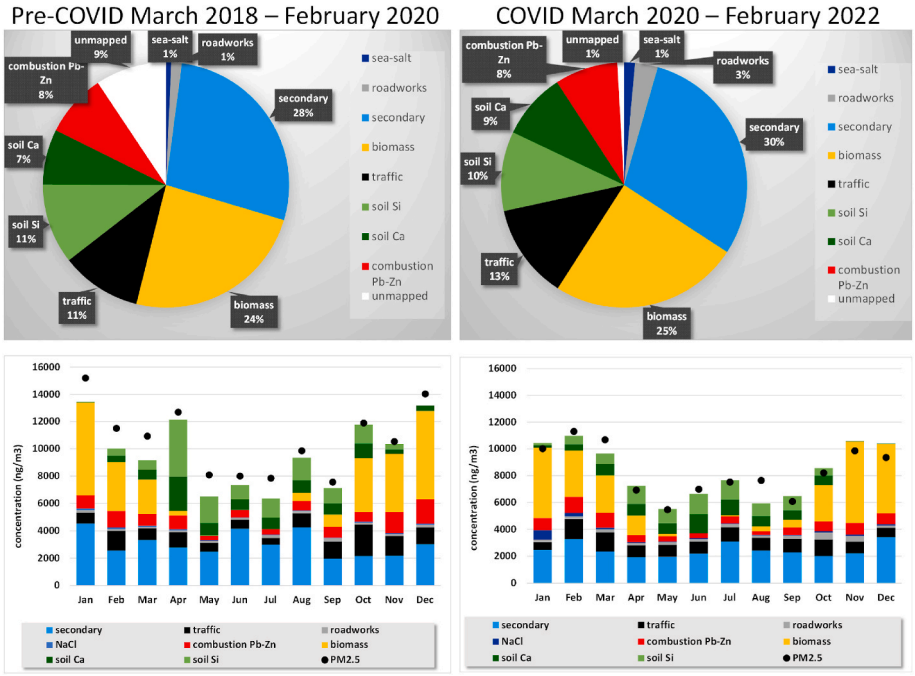

Fig. 6. Source contributions of $PM_{2.5}$ before and during COVID-19 pandemic.

It is characterized by a high sulfur content. Fossil fuel combustion is the primary source of various compounds of SO_4^{-2} (Chow and Watson, 2002). V and Ni, the fingerprint elements of heavy oil combustion, are also present in this factor. Secondary sulphate accounted for 28–30% of the $PM_{2.5}$ mass. Its contribution was relatively evenly distributed throughout the year. Secondary sulphate has a residence time of 2–10 days (Bondietti and Papastefanou, 1993) which allows regional and long-range transport. PSCF and CWT analysis showed that the source areas of secondary sulphate pollution in Debrecen were the industrial regions of SW Romania, the Balkan countries, and occasionally western Ukraine and southern Poland, as shown in Fig. 7. These are the areas of high SO_2 emission fluxes in the OMI-HTAP SO_2 inventory (Fioletov et al., 2016; Liu et al., 2018), as shown in Fig. S13.

The factor named 'Biogenic emission' was a significant source of PM_{coarse}, with a 19% yearly average contribution. The characteristic components of this factor were P and K, which are essential elements for plants. Therefore, this factor is attributed to the emission of primary biogenic aerosols like plant debris. This source was dominant in the vegetation period, with maximums in the summer. Primary biological organic aerosols (PBOA) is a major component of the coarse fraction (Samaké et al., 2020; Szidat et al., 2006), during the vegetation period its contribution can be up to 50%. Studies based on aerosol mass spectrometry (Samaké et al., 2020) and C-14 analysis (Salma et al., 2020a,b) showed that over 60% of organic matter has biogenic origin in summer,

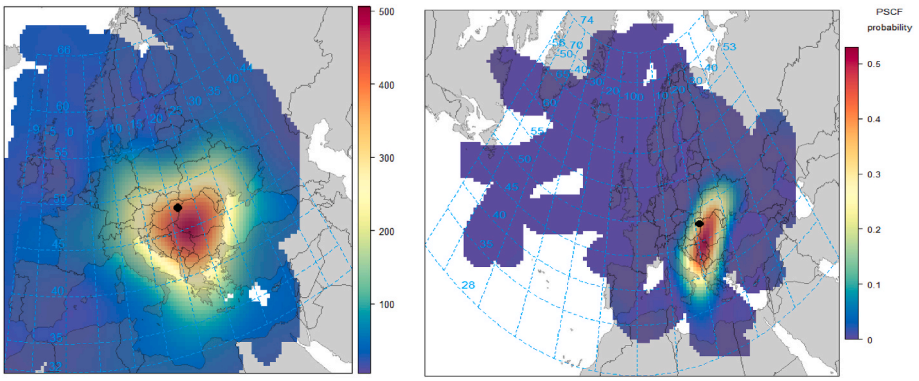

Fig. 7. Results of CWT (left) and PSCF (threshold: 75%) (right) of S in $PM_{2.5}$ for summers 2018–2019.

while in winter primary and secondary biogenic aerosols still could have a contribution up to 20% for OM in PM10. This is consistent with our findings.

The factor containing Mn, soil dust elements and metals is apportioned to road works in both size fractions. This was a temporary source from 2021, when big road reconstructions were running in the neighboring main roads together with the replacement of tram line rails. In PM_{coarse}, a factor identified as construction/building is also present. This can be connected to the construction of a tower block, as mentioned earlier in Section 2.2 in connection with Cl. This is a mixed source of construction and salt. The factor containing 90% of the fine fraction Na and Cl is identified as sea salt. The contribution of these sources was a few percent, and they are only present periodically.

Figs. 5 and 6 show, that considering a whole year there was basically no change in the relative contribution of sources, with the exception of temporary sources like construction and roadworks. In both fractions, the seasonal variation was similar in the two investigated periods; however, the differences became smaller during the years of the pandemic. The high concentrations of soil factors in April pre-COVID originated from several Saharan dust episodes. In March and April 2020 earthworks were carried out over a large area in preparation for the BMW factory, which is located 10 km to the north-west, which was the prevailing wind direction in March 2020. In October, in the pre-COVID years, an elevated contribution of soil can be seen. The most probable explanation for this is the lack of precipitation this month in 2018 and 2019 and increased agricultural activity, as explained earlier in connection with the BC timeline. Changes related to lockdowns and relaxation periods will be discussed in detail in the next section.

3.4. COVID crisis induced changes in $PM_{2.5}$, PM_{coarse}, composition and sources

Relative changes in $PM_{2.5}$, PM_{coarse}, elemental components and source contributions over the studied time periods are presented in Figs. 8 and 9. Species for which the change was significant according to the Mann-Whitney-U test are marked with an asterix. Considering the whole time period, concentrations of $PM_{2.5}$, PM_{coarse} and PM_{10} were 25%, 20% and 22% less, respectively, during the years of the pandemic than the corresponding baseline values.

In the coarse fraction, a significant decrease could be observed for almost all elemental components, with a few exceptions. Mineral dust components and soil factors decreased by 30% on average. In the case of traffic related elements and source, the decrease was more than 40%. Biogenic emission was also decreased by 30%, which could be attributed to the decrease in agricultural activity on the surrounding land and to the reduced resuspension of biogenic aerosols due to traffic.

In the case of $PM_{2.5}$, significant changes were recorded only for traffic related elemental components like Cu and Zn. In the case of BC and S, the change was significant only for summer (25% increase for BC and 35% decrease for S). Source contributions decreased by 10–30% in average, apart from the periodic sources of sea salt and roadworks.

Looking at the periods separately, it is striking that the first, most strict closure did not result in a significant decrease in the concentration of pollutants, whereas during the relaxation period of 2020, the decrease was 30–50% for almost all components. In the case of the first lockdown, March–May 2020, there was an increase in the concentration of some soil related elements, BC and K. In both size fractions, the contribution of soil Ca, biomass burning, combustion and roadworks increased considerably compared to the same period in the previous 2 years. In March and April, earthworks were carried out on the BMW construction site in the prevailing wind direction, there were Saharan and Asian dust episodes; the average temperature of the spring of 2020 was 1.5 °C cooler, and the air was less humid (by ~10%) than in the previous years (Table 2). In addition, people were forced to stay at home during the day, so more heating was needed. Furthermore, car traffic also increased in residential areas. Thus, the combined effect of meteorology, desert dust storms, intense construction works, and the change in the lifestyle of the population caused the anomaly observed in the first lockdown.

In summer and autumn 2020, the amount of precipitation was 2–2.5 times higher than the baseline value. The wet weather could cause the large reduction of PM and its components in the coarse fraction, whereas the decrease was smaller in the fine fraction, which is less affected by the precipitation. In this period, an increase could be observed only in the case of BC originating from vehicle exhaust emission and thus traffic source contribution to $PM_{2.5}$.

In summer 2021, when the weather was warm and dry, mineral dust and traffic components, as well as the source contributions, were similar or higher than the baseline values. The huge increase in fine fraction soil contribution could be attributed to the restarted construction of the BMW factory. In the 3rd quarter of 2021, the construction of the infrastructure took place, which involved moving a large amount of earth. This effect was more significant in the fine fraction because of the distance from the construction site (10 km).

This time, the significant decrease in secondary sulphate concentration caused the ~20% lower $PM_{2.5}$ concentration values. Somewhat lower concentration values compared to baseline were found in September–October 2021, which was followed by a decrease in traffic and soil source contributions; however, its extent was less than in the rainy year of 2020. The reduced biogenic emission and reduced P concentrations indicate reduced agricultural activity, too. It should be noted that due to the construction of the BMW industrial site the size of the high-quality agricultural land in the prevailing wind direction has been significantly reduced.

In November 2020, the number of COVID cases was increasing significantly, therefore, even before the lockdown, people stayed at home and tried to keep social distancing. This resulted in very similar concentration levels and source contributions to the lockdowns that followed. During winter 2020-21 and spring 2021, i.e., lockdown2 and

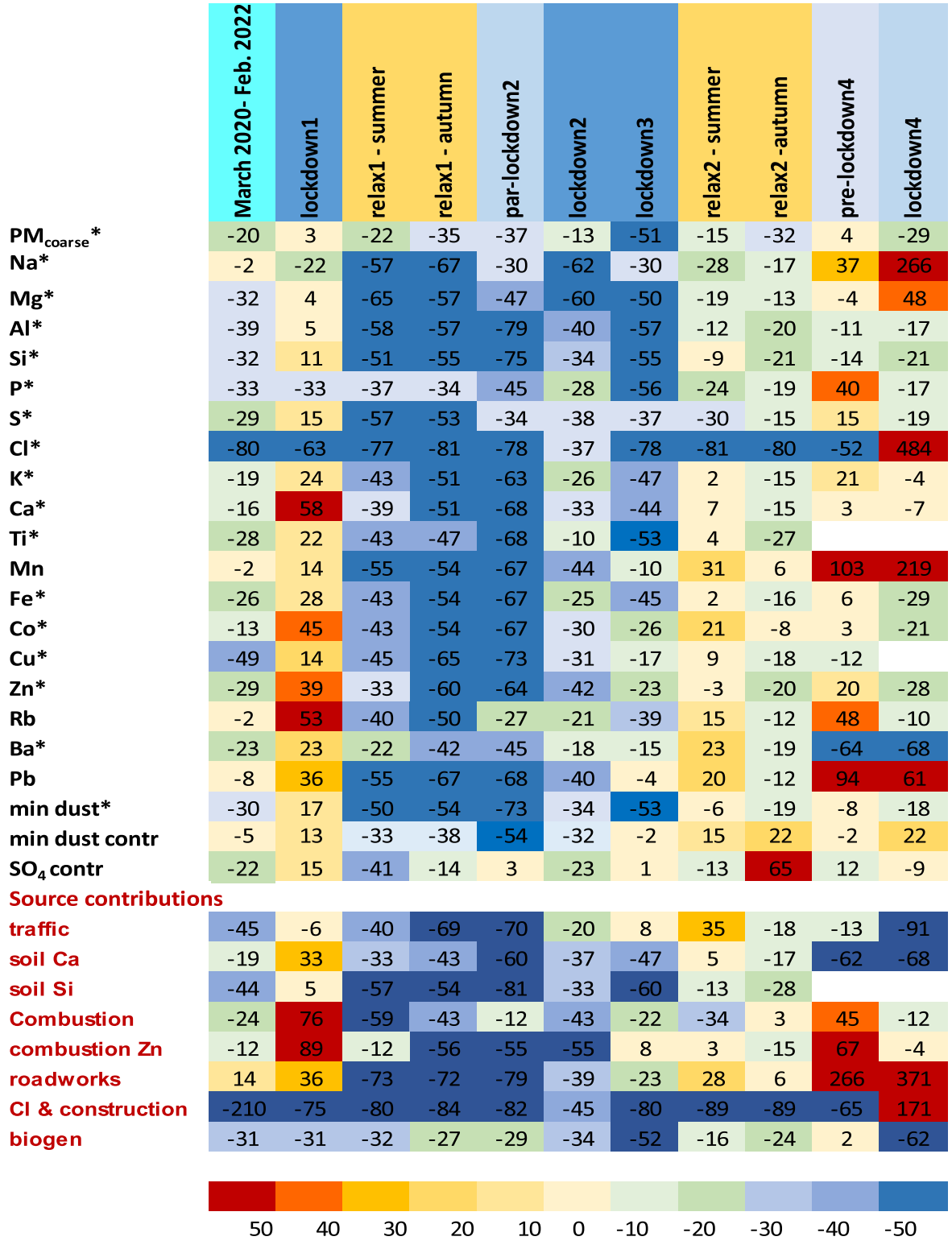

Fig. 8. Relative change (%) of PM_{coarse}, components and source contributions.

lockdown3, basically what happened was what was expected: a reduction in most components compared to the baseline. The extent of the reduction was smaller during lockdown2, when schools and workplaces were still open. The milder weather conditions could cause the smaller contribution from heating (biomass and combustion). During lockdown3, in spring 2021, we experienced the highest reduction of air pollutants in all AQ monitoring points in the city, except at the hospital. The coarse PM and mineral dust components were reduced by 50–60%, while the $PM_{2.5}$ concentration decreased by 33%. At the same time, the contribution of domestic heating increased considerably due to the cold weather conditions and the fact that people had to stay at home during the day, too. The contribution of traffic did not change significantly.

In November 2021, the meteorological situation was in favor of the development of high pollution level episodes with very low boundary

	March 2020- Feb. 2022	lockdown1	relax1 - summer	relax1 - autumn	par-lockdown2	lockdown2	lockdown3	relax2 - summer	relax2 -autumn	pre-lockdown4	lockdown4
PM_{10}*	-22	-6	-18	-37	-28	-11	-43	-19	-26	13	-25
$PM_{2.5}$*	-25	-16	-13	-40	-24	-10	-33	-21	-19	18	-24
BC	-19	45	54	-43	-23	-16	-3	-3	-20	31	-23
Na*	15	-22	-32	-60	-8	-26	-40	5	-12	32	284
Mg	3	1	-30	-45	-16	4	-64	35	31	-14	160
Al	-17	-5	-37	-46	-57	-19	-68	36	7	-5	-2
Si	-12	4	-30	-41	-51	-15	-65	30	5	-4	-10
P*	-9	-9	-15	6	-12	-26	-42	-37	-8	117	21
S	-19	-14	-37	-8	6	-7	-13	-23	9	26	1
K	-15	22	-20	-55	-23	-20	-17	7	21	76	17
Ca	10	54	-6	-36	-51	-9	-50	45	12	8	2
Ti	-12	10	-30	-26	-61	-3	-65	32	-19		
Mn*	26	13	21	1	7	4	25	62	92	174	89
Fe*	-6	22	-18	-40	-38	-12	-44	26	6	24	-16
Cu*	-23	-35	-14	-42	-24	3	-30	4	5	-27	-44
Zn*	-23	11	-23	-45	-29	-15	-6	1	-2	27	-6
Ba	7	11	11	-30	-27	5	-2	48	35	-69	-22
Pb	-14	1	-24	-37	-16	-11	-4	-5	5	57	25
min. dust	-9	14	-27	-41	-48	-21	-62	32	7	3	-4
min dust contr	17	27	4	-6	-37	-3	-34	50	27	-6	45
SO_4 contr	17	1	-13	50	23	20	33	6	46	10	47
BC contr	13	83	118	-9	2	-8	49	49	-12	15	0
Source contributions											
traffic	-12	16	73	-40	-33	14	7	-9	-38	-45	-67
soil Ca	-10	59	1	-39	-86	1	-59	58	-16	-104	-56
soil Si	-29	-9	-47	-47	-84		-74	29	-21		-34
biomass	-26	115		-68	-18	-32	49		-15	93	5
combustion Pb-Zn	-28	-6	-43	-36	-43	-17	-1	7	6	4	-30
roadworks	48	28	-25	-2	-4	2	47	41	230	307	132
(sea)salt	44	-10	-14	-56	26	-21	-9	10	22	91	545
secondary	-21	-42	-39	19	34	22	-13	-33	0	35	-16

50 40 30 20 10 0 -10 -20 -30 -40 -50

Fig. 9. Relative change (%) of $PM_{2.5}$, components and source contributions.

layer and mixing layer heights, low wind speed, and low temperatures. As a result, higher concentrations were measured compared to the baseline, especially in $PM_{2.5}$. Most of the pollution originated from domestic heating and road construction at this time.

In winter 2021-22, PM levels were 25% lower on average than the baseline. This time there were almost no restrictions due to COVID, and life was back to 'normal', therefore pollution levels similar to baseline were expected. In addition, meteorological conditions led towards more high pollution episodes, as happened in November previously. The explanation might lie in the appearance of sea salt in the air of Debrecen. Fig. 10 shows the cluster means for the whole investigated period, for all winters from 2018 to 2022, and for lockdown4.

Usually, air masses arrive in Debrecen from W, NW direction in 30% of cases. That winter, this number was over 70%. In addition, trajectories from Romania were missing. Average PM concentrations and source contributions are summarized in Table 5 for each of the 5 trajectory clusters for December 2021–February 2022. The results shows that air masses of oceanic origin (clusters 3 and 4) were associated with very low $PM_{2.5}$ concentrations and high sea-salt source contributions (25–38%), whereas trajectories of eastern European origin (cluster 5) resulted very high pollution levels. It seems that in winter of 2021-22 clean air masses of oceanic origin influenced the air above Debrecen, resulting in low air pollution levels and a high sea salt content of APM.

Air pollution originating from long range and regional transport plays an important role in the evolution of the air quality of the city. One of the main components of $PM_{2.5}$ is secondary sulphate. In the source contribution of secondary sulphate aerosol, a significant decrease was detected in spring and summer 2020 and in summer 2021. CWT calculations showed that the source areas of sulfur were SW Romania and the Balkan countries during the 4-year-long investigated period (see Fig. S14 in Supplementary Materials); therefore, we could conclude that there was a significant decrease in SO_2 emission in the source areas. In autumn 2020, the contribution of secondary aerosols increased compared to baseline. PSCF analysis (Fig. 11) revealed that the Po-Valley region was the source of the increased S concentration.

4. Summary and conclusions

In this work, the variation of air pollution was investigated in a central-eastern European city during lockdowns due to the COVID-19 pandemic compared to the previous two years.

In order to understand all the processes that influenced the evolution of air pollution in the city, we have introduced an integrated approach which combines receptor modelling, trajectory statistical methods, and local and regional meteorology taking into account anthropogenic activities. With this study, we have demonstrated the robustness of this methodology; therefore, it can serve as a guide for future studies.

Concentration, composition, and sources of $PM_{2.5}$ and PM_{coarse} were determined at an urban background site in Debrecen, Hungary, from March 2018 to March 2022. The time interval included 4 lockdowns, 2 transition and 2 relaxation periods, which were also studied individually.

Source apportionment by PMF identified 8 sources, both in the fine and coarse fractions. These were: soil dust, combustion, biomass burning, biogenic emission, traffic, secondary sulphate, sea salt, construction and roadworks. In the heating season, biomass burning and combustion from heating were the main sources of pollution, while in the summer, besides soil dust, secondary aerosols and biogenic emission gave the highest contribution in $PM_{2.5}$ and PM_{coarse}, respectively.

From March 2020, the restrictions due to the pandemic influenced strongly the concentration of all air pollutants in all AQ monitoring points of the city. Considering the whole 2-year period of COVID-19, a 20% reduction in average could be detected in the case of most gaseous and APM pollutants and in the components and sources of $PM_{2.5}$ and PM_{coarse}. In the coarse fraction, the contribution of traffic and soil, most of which is resuspended dust due to traffic, decreased to the greatest

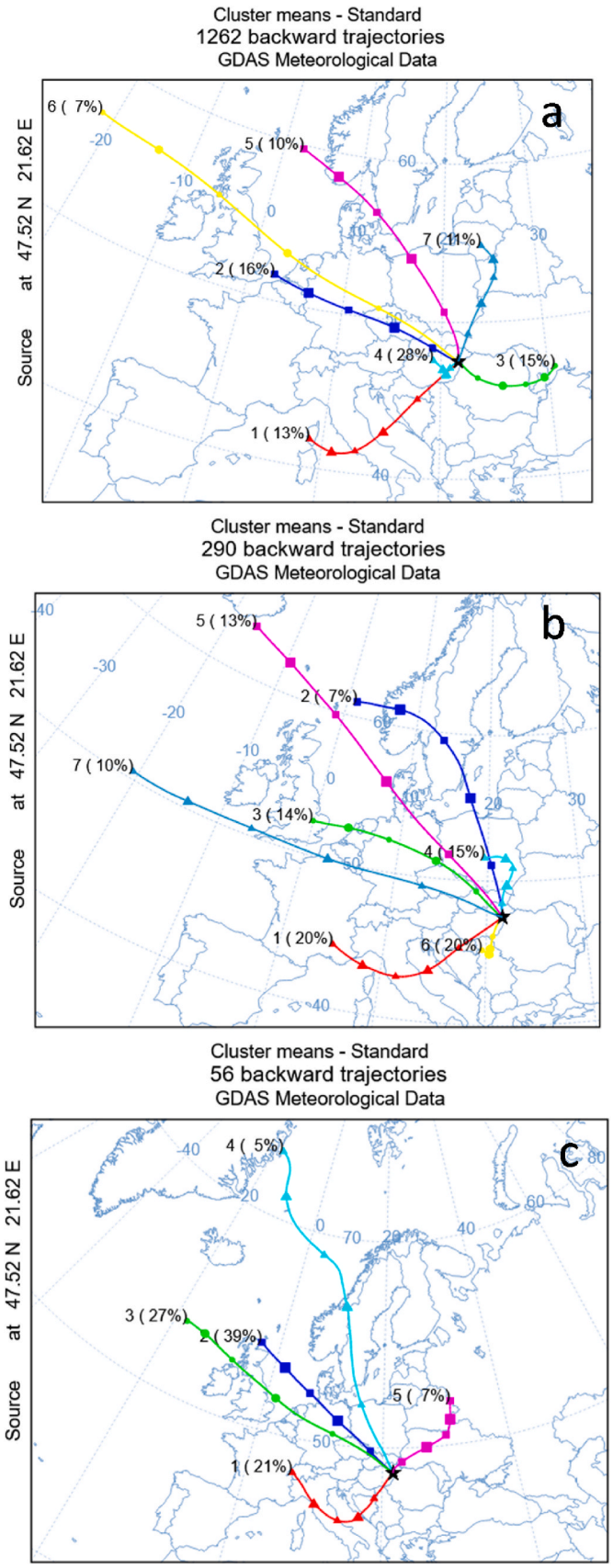

Fig. 10. Cluster means of backward trajectories calculated by trajectory clustering in HYSPLIT for the whole period of March 2018–February 2022 (a), for winters 2018–2022 (b) and December 2021–February 2022 (c).

Table 5
Average $PM_{2.5}$, PM_{coarse}, PM_{10} concentrations and source contributions in $\mu g/m^3$ for trajectory clusters between December 2021–February 2022.

	cluster	1	2	3	4	5
	$PM_{2.5}$	8.99	10.9	3.27	3.45	26.9
	PM_{coarse}	3.55	3.7	3.31	2.66	11.2
	PM_{10}	12.5	14.6	6.58	6.10	38.1
$PM_{2.5}$ source contributions	**NaCl**	0.12	0.79	0.77	0.85	1.01
	roadworks	0.28	0.20	0.36	0.35	0.33
	secondary	3.40	2.48	0.38	1.19	5.87
	biomass	5.65	5.99	1.20	1.55	18.2
	traffic	0.50	0.49	0.01	0.02	2.21
	combustion	1.07	1.31	0.01	0.13	1.00
	Pb–Zn soil	0.23	0.14	0.34	0.17	1.63
PM_{coarse} source contributions	**combustion Zn**	0.38	0.26	0.09	0.10	0.82
	roadworks	0.90	1.05	0.98	0.99	2.52
	Cl salts	0.27	0.69	1.17	1.27	0.00
	traffic	0.20	0.07	0.01	0.01	0.00
	combustion	0.67	0.80	0.14	0.09	2.18
	biogen	0.32	0.25	0.07	0.01	1.37
	soil	0.88	0.01	0.76	0.01	2.60

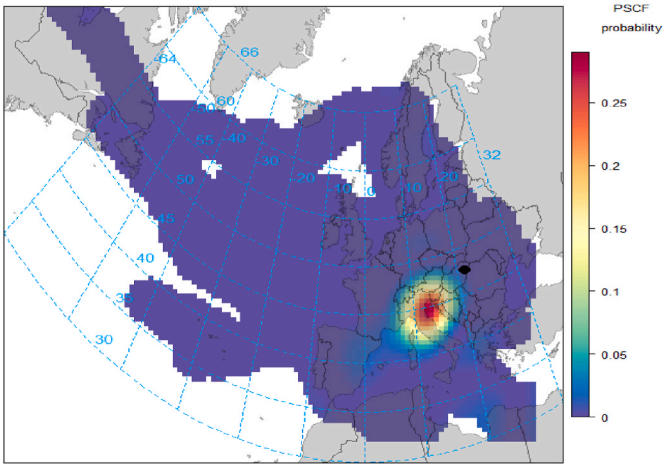

Fig. 11. Result of PSCF calculation for secondary sulphate in September–November 2020.

extent. A significant reduction in agricultural activities around the city could also be traced back. In $PM_{2.5}$ sources related to energy production decreased the most. However, during the closures in the springs of 2020 and 2021, a significant increase in biomass burning from domestic heating was detected, which was caused by the forced staying at home and the colder weather. The shift of traffic-related pollutants from the school year to the summer relaxation periods is also an indication of the changed habits of the urban population.

Another important local source was construction and roadworks, which intensified from time to time during the 4 years of the study. The impact of a large-scale industrial site development on the concentration and composition of $PM_{2.5}$ could be identified even from a distance of up to 10 km.

We have shown that a large part of APM pollution in Debrecen comes from regional and long-range transport. The main source areas of secondary sulphate aerosols were the western Balkan countries and southwest Romania. Therefore, the change in emission in these countries also had a strong influence on the air pollution level in the city.

When investigating the lockdown, transition, and relaxation periods individually, the picture becomes rather complex. Local meteorological parameters, the origin of air masses, and long-range transport processes had a significant influence on the evolution of air pollution in the 2-3-month time intervals. The effects of these conditions were similar in magnitude to the changes caused by the closures. These parameters could cancel out, reverse, or amplify the effects of the restrictions, as we have seen, e.g., for lockdown1 and lockdown4. Therefore, when investigating such short time periods, all possible circumstances must be taken into consideration in order to reach the right conclusions. Averaging over a sufficiently long time period – 2 years in our case – these short-term effects are smoothed out.

Atmospheric particulate matter pollution is a severe problem in all urban environments around the world. Therefore, the reduction of APM exposure is a primary goal of the authorities.

Thanks to the special situation due to the COVID-19 pandemic, we have shown that a significant reduction in traffic and industrial production locally and globally could improve the air quality of an east-central European city by 20–25% in the long term. The results of source apportionment indicated that only properly targeted local and regional measures together would provide a reduction of urban air pollution to the required level. We have also shown the importance of understanding the effects of complex local and global meteorological situations and episodic emissions from distant natural and anthropogenic sources. All our results point in the direction that AQ improvement policies in the future should be based on source apportionment, which takes into account local, regional, and global influences of meteorological parameters and emission sources.

CRediT authorship contribution statement

Zsófia Kertész: Conceptualization, Data curation, Formal analysis, Investigation, Methodology, Resources, Supervision, Validation, Visualization, Writing – original draft, Writing – review & editing. **Shafa Aljboor:** Formal analysis, Investigation, Writing – original draft, Writing – review & editing. **Anikó Angyal:** Formal analysis, Investigation, Writing – review & editing. **Enikő Papp:** Formal analysis, Investigation, Writing – review & editing. **Enikő Furu:** Investigation, Writing – review & editing. **Máté Szarka:** Investigation, Writing – review & editing. **Sándor Bán:** Investigation, Validation, Writing – review & editing. **Zita Szikszai:** Writing – review & editing.

Declaration of competing interest

The authors declare that they have no known competing financial interests or personal relationships that could have appeared to influence the work reported in this paper.

Data availability

Data will be made available on request.

Acknowledgements

The research was supported by the grant GINOP-2.3.3-15-2016-00005.

Dust data and images were provided by the WMO Barcelona Dust Regional Center and the partners of the Sand and Dust Storm Warning Advisory and Assessment System (SDS-WAS) for Northern Africa, the Middle East and Europe. The authors gratefully acknowledge the NOAA Air Resources Laboratory (ARL) for the provision of the HYSPLIT transport and dispersion model used in this publication.

Appendix A. Supplementary data

Supplementary data to this article can be found online at https://doi.org/10.1016/j.atmosenv.2023.120267.

References

AboutHungary. (n.d.). https://abouthungary.hu/.

Aljboor, S., Angyal, A., Baranyai, D., Papp, E., Szarka, M., Szikszai, Z., Rajta, I., Vajda, I., Kertész, Z., 2023. Light-element sensitive in-air millibeam PIXE setup for fast measurement of atmospheric aerosol samples. J. Anal. Atomic Spectrom. 38 (1), 57–65. https://doi.org/10.1039/D2JA00291D.

Almeida, S.M., Manousakas, M., Diapouli, E., Kertesz, Z., Samek, L., Hristova, E., Šega, K., Alvarez, R.P., Belis, C.A., Eleftheriadis, K., 2020. Ambient particulate matter source apportionment using receptor modelling in European and Central Asia urban areas. Environ. Pollut. 266, 115199 https://doi.org/10.1016/j.envpol.2020.115199.

Angyal, A., Ferenczi, Z., Manousakas, M., Furu, E., Szoboszlai, Z., Török, Z., Papp, E., Szikszai, Z., Kertész, Z., 2021. Source identification of fine and coarse aerosol during smog episodes in Debrecen, Hungary. Air Quality, Atmosphere & Health 14 (7), 1017–1032. https://doi.org/10.1007/s11869-021-01008-8.

Angyal, A., Kertész, Zs, Szikszai, Z., Szoboszlai, Z., 2010. Study of Cl-containing urban aerosol particles by ion beam analytical methods. Nucl. Instrum. Methods Phys. Res. Sect. B Beam Interact. Mater. Atoms 268 (11–12), 2211–2215. https://doi.org/10.1016/j.nimb.2010.02.090.

Bakola, M., Hernandez Carballo, I., Jelastopulu, E., Stuckler, D., 2022. The impact of COVID-19 lockdown on air pollution in Europe and North America: a systematic review. Eur. J. Publ. Health 32 (6), 962–968. https://doi.org/10.1093/eurpub/ckac118.

Bao, R., Zhang, A., 2020. Does lockdown reduce air pollution? Evidence from 44 cities in northern China. Sci. Total Environ. 731, 139052 https://doi.org/10.1016/j.scitotenv.2020.139052.

Berman, J.D., Ebisu, K., 2020. Changes in U.S. air pollution during the COVID-19 pandemic. Sci. Total Environ. 739, 139864 https://doi.org/10.1016/j.scitotenv.2020.139864.

Bondietti, E.A., Papastefanou, C., 1993. Estimates of residence times of sulfate aerosols in ambient air. Sci. Total Environ. 136 (1–2), 25–31. https://doi.org/10.1016/0048-9697(93)90294-G.

Borbély-Kiss, I., Koltay, E., Szabó, G.Y., Bozó, L., Tar, K., 1999. Composition and sources of urban and rural atmospheric aerosol in eastern Hungary. J. Aerosol Sci. 30 (3), 369–391. https://doi.org/10.1016/S0021-8502(98)00051-2.

Borkowski, P., Jażdżewska-Gutta, M., Szmelter-Jarosz, A., 2021. Lockdowned: everyday mobility changes in response to COVID-19. J. Transport Geogr. 90, 102906 https://doi.org/10.1016/j.jtrangeo.2020.102906.

Briz-Redón, Á., Belenguer-Sapiña, C., Serrano-Aroca, Á., 2021. Changes in air pollution during COVID-19 lockdown in Spain: a multi-city study. J. Environ. Sci. 101, 16–26. https://doi.org/10.1016/j.jes.2020.07.029.

Brown, S.G., Eberly, S., Paatero, P., Norris, G.A., 2015. Methods for estimating uncertainty in PMF solutions: examples with ambient air and water quality data and guidance on reporting PMF results. Sci. Total Environ. 518–519, 626–635. https://doi.org/10.1016/j.scitotenv.2015.01.022.

Bucsky, P., 2020. Modal share changes due to COVID-19: the case of Budapest. Transp. Res. Interdiscip. Perspect. 8, 100141 https://doi.org/10.1016/j.trip.2020.100141.

Campbell, J.L., Boyd, N.I., Grassi, N., Bonnick, P., Maxwell, J.A., 2010. The Guelph PIXE software package IV. Nucl. Instrum. Methods Phys. Res. Sect. B Beam Interact. Mater. Atoms 268 (20), 3356–3363. https://doi.org/10.1016/j.nimb.2010.07.012.

Carslaw, D.C., Ropkins, K., 2012. Openair — an R package for air quality data analysis. Environ. Model. Software 27 (28), 52–61. https://doi.org/10.1016/j.envsoft.2011.09.008.

Chow, J.C., Watson, J.G., 2002. Review of PM $_{2.5}$ and PM $_{10}$ apportionment for fossil fuel combustion and other sources by the chemical mass balance receptor model. Energy Fuels 16 (2), 222–260. https://doi.org/10.1021/ef0101715.

Clemente, Á., Yubero, E., Nicolás, J.F., Caballero, S., Crespo, J., Galindo, N., 2022. Changes in the concentration and composition of urban aerosols during the COVID-19 lockdown. Environ. Res. 203, 111788 https://doi.org/10.1016/j.envres.2021.111788.

Cohen, D.D., Atanacio, A., Crawford, J., Siegele, R., 2020. Ion beam techniques for source fingerprinting fine particle air pollution in major Asian-Pacific cities. Nucl. Instrum. Methods Phys. Res. Sect. B Beam Interact. Mater. Atoms 477, 122–132. https://doi.org/10.1016/j.nimb.2019.07.023.

Di Gilio, A., de Gennaro, G., Dambruoso, P., Ventrella, G., 2015. An integrated approach using high time-resolved tools to study the origin of aerosols. Sci. Total Environ. 530–531, 28–37. https://doi.org/10.1016/j.scitotenv.2015.04.073.

Dobos, E., Borbély-Kiss, I., Kertész, Zs, Szabó, Gy, Koltay, E., 2009. Debrecen, Hungary on the fine-fraction aerosol map of Europe. J. Radioanal. Nucl. Chem. 279 (1), 143–157. https://doi.org/10.1007/s10967-007-7207-y.

EEA. Classification of monitoring stations and criteria to include them in EEA's assessments products (n.d.-a). https://www.eea.europa.eu/themes/air/air-quality-concentrations/classification-of-monitoring-stations-and. (Accessed 21 November 2023).

EEA. EU air quality standards (n.d.-b). https://environment.ec.europa.eu/topics/air/air-quality/eu-air-quality-standards_en.

Fioletov, V.E., McLinden, C.A., Krotkov, N., Li, C., Joiner, J., Theys, N., Carn, S., Moran, M.D., 2016. A global catalogue of large SO2 sources and emissions derived from the Ozone Monitoring Instrument. Atmos. Chem. Phys. 16 (18), 11497–11519. https://doi.org/10.5194/acp-16-11497-2016.

Furu, E., Angyal, A., Szoboszlai, Z., Papp, E., Török, Z., Kertész, Z., 2022. Characterization of aerosol pollution in two Hungarian cities in winter 2009–2010. Atmosphere 13 (4), 554. https://doi.org/10.3390/atmos13040554.

Gamelas, C.A., Canha, N., Vicente, A., Silva, A., Borges, S., Alves, C., Kertesz, Z., Almeida, S.M., 2023. Source apportionment of PM2.5 before and after COVID-19 lockdown in an urban-industrial area of the Lisbon metropolitan area, Portugal. Urban Clim. 49, 101446 https://doi.org/10.1016/j.uclim.2023.101446.

Ghahremanloo, M., Lops, Y., Choi, Y., Mousavinezhad, S., 2021. Impact of the COVID-19 outbreak on air pollution levels in East Asia. Sci. Total Environ. 754, 142226 https://doi.org/10.1016/j.scitotenv.2020.142226.

Giardi, F., Nava, S., Calzolai, G., Pazzi, G., Chiari, M., Faggi, A., Andreini, B.P., Collaveri, C., Franchi, E., Nincheri, G., Amore, A., Becagli, S., Severi, M., Traversi, R., Lucarelli, F., 2022. PM $_{10}$ variation, composition, and source analysis in Tuscany (Italy) following the COVID-19 lockdown restrictions. Atmos. Chem. Phys. 22 (15), 9987–10005. https://doi.org/10.5194/acp-22-9987-2022.

Google. COVID-19 community mobility reports. https://www.google.com/covid19/mobility/. (Accessed 10 June 2023).

Hale, T., Angrist, N., Goldszmidt, R., Kira, B., Petherick, A., Phillips, T., Webster, S., Cameron-Blake, E., Hallas, L., Majumdar, S., Tatlow, H., 2021. A global panel database of pandemic policies (Oxford COVID-19 Government Response Tracker). Nat. Human Behav. 5 (4), 529–538. https://doi.org/10.1038/s41562-021-01079-8.

Hersbach, H., Bell, B., Berrisford, P., Hirahara, S., Horányi, A., Muñoz-Sabater, J., Nicolas, J., Peubey, C., Radu, R., Schepers, D., Simmons, A., Soci, C., Abdalla, S., Abellan, X., Balsamo, G., Bechtold, P., Biavati, G., Bidlot, J., Bonavita, M., et al., 2020. The ERA5 global reanalysis. Q. J. R. Meteorol. Soc. 146 (730), 1999–2049. https://doi.org/10.1002/qj.3803.

Hersbach, H., Bell, B., Berrisford, P., Biavati, G., Horányi, A., Muñoz Sabater, J., Nicolas, J., Peubey, C., Radu, R., Rozum, I., Schepers, D., Simmons, A., Soci, C., Dee, D., Thépaut, J.-N., 2023. ERA5 hourly data on single levels from 1940 to present. In: Copernicus Climate Change Service (C3S) Climate Data Store (CDS). https://doi.org/10.24381/cds.adbb2d47, 01-JUN-2023.

Higham, J.E., Ramírez, C.A., Green, M.A., Morse, A.P., 2021. UK COVID-19 lockdown: 100 days of air pollution reduction? Air Quality, Atmosphere & Health 14 (3), 325–332. https://doi.org/10.1007/s11869-020-00937-0.

Hopke, P.K., 2016. Review of receptor modeling methods for source apportionment. J. Air Waste Manag. Assoc. 66 (3), 237–259. https://doi.org/10.1080/10962247.2016.1140693.

Hopke, P.K., Xie, Y., Raunemaa, T., Biegalski, S., Landsberger, S., Maenhaut, W., Artaxo, P., Cohen, D., 1997. Characterization of the gent stacked filter unit PM $_{10}$ sampler. Aerosol. Sci. Technol. 27 (6), 726–735. https://doi.org/10.1080/02786829708965507.

Hudda, N., Simon, M.C., Patton, A.P., Durant, J.L., 2020. Reductions in traffic-related black carbon and ultrafine particle number concentrations in an urban neighborhood during the COVID-19 pandemic. Sci. Total Environ. 742, 140931 https://doi.org/10.1016/j.scitotenv.2020.140931.

Ivanovski, M., Lavrič, P.D., Vončina, R., Goričanec, D., Urbancl, D., 2022. Improvement of air quality during the COVID-19 lockdowns in the republic of Slovenia and its connection with meteorology. Aerosol Air Qual. Res. 22 (9), 210262 https://doi.org/10.4209/aaqr.210262.

Jeong, C.-H., Yousif, M., Evans, G.J., 2022. Impact of the COVID-19 lockdown on the chemical composition and sources of urban PM2.5. Environ. Pollut. 292, 118417 https://doi.org/10.1016/j.envpol.2021.118417.

Kalogridis, A.-C., Vratolis, S., Liakakou, E., Gerasopoulos, E., Mihalopoulos, N., Eleftheriadis, K., 2018. Assessment of wood burning versus fossil fuel contribution to wintertime black carbon and carbon monoxide concentrations in Athens, Greece. Atmos. Chem. Phys. 18 (14), 10219–10236. https://doi.org/10.5194/acp-18-10219-2018.

Kar, S., Maity, J.P., Samal, A.C., Santra, S.C., 2010. Metallic components of traffic-induced urban aerosol, their spatial variation, and source apportionment. Environ. Monit. Assess. 168 (1–4), 561–574. https://doi.org/10.1007/s10661-009-1134-z.

Kertész, Zs, Szoboszlai, Z., Angyal, A., Dobos, E., Borbély-Kiss, I., 2010. Identification and characterization of fine and coarse particulate matter sources in a middle-European urban environment. Nucl. Instrum. Methods Phys. Res. Sect. B Beam Interact. Mater. Atoms 268 (11–12), 1924–1928. https://doi.org/10.1016/j.nimb.2010.02.103.

Liu, F., Choi, S., Li, C., Fioletov, V.E., McLinden, C.A., Joiner, J., Krotkov, N.A., Bian, H., Janssens-Maenhout, G., Darmenov, A.S., da Silva, A.M., 2018. A new global anthropogenic SO2 emission inventory for the last decade: a mosaic of satellite-derived and bottom-up emissions. Atmos. Chem. Phys. 18 (22), 16571–16586. https://doi.org/10.5194/acp-18-16571-2018.

Maenhaut, W., 2015. Present role of PIXE in atmospheric aerosol research. Nucl. Instrum. Methods Phys. Res. Sect. B Beam Interact. Mater. Atoms 363, 86–91. https://doi.org/10.1016/j.nimb.2015.07.043.

Major, I., Furu, E., Varga, T., Horváth, A., Futó, I., Gyökös, B., Somodi, G., Lisztes-Szabó, Z., Jull, A.J.T., Kertész, Z., Molnár, M., 2021. Source identification of PM2.5 carbonaceous aerosol using combined carbon fraction, radiocarbon and stable carbon isotope analyses in Debrecen, Hungary. Sci. Total Environ. 782, 146520 https://doi.org/10.1016/j.scitotenv.2021.146520.

Manchanda, C., Kumar, M., Singh, V., Faisal, M., Hazarika, N., Shukla, A., Lalchandani, V., Goel, V., Thamban, N., Ganguly, D., Tripathi, S.N., 2021. Variation in chemical composition and sources of PM2.5 during the COVID-19 lockdown in Delhi. Environ. Int. 153, 106541 https://doi.org/10.1016/j.envint.2021.106541.

Manisalidis, I., Stavropoulou, E., Stavropoulos, A., Bezirtzoglou, E., 2020. Environmental and health impacts of air pollution: a review. Front. Public Health 8. https://doi.org/10.3389/fpubh.2020.00014.

Manohar, M., Atanacio, A., Button, D., Cohen, D., 2021. Mabi - a multi-wavelength absorption black carbon instrument for the measurement of fine light absorbing carbon particles. Atmos. Pollut. Res. 12 (4), 133–140. https://doi.org/10.1016/j.apr.2021.02.009.

Massimi, L., Pietrodangelo, A., Frezzini, M.A., Ristorini, M., De Francesco, N., Sargolini, T., Amoroso, A., Di Giosa, A., Canepari, S., Perrino, C., 2022. Effects of COVID-19 lockdown on PM10 composition and sources in the Rome Area (Italy) by

elements' chemical fractionation-based source apportionment. Atmos. Res. 266, 105970 https://doi.org/10.1016/j.atmosres.2021.105970.
Mathieu, E., et al.. Coronavirus pandemic (COVID-19). Published Online at. https://ourworldindata.org/coronavirus. (Accessed 20 May 2023).
Menut, L., Bessagnet, B., Siour, G., Mailler, S., Pennel, R., Cholakian, A., 2020. Impact of lockdown measures to combat Covid-19 on air quality over western Europe. Sci. Total Environ. 741, 140426 https://doi.org/10.1016/j.scitotenv.2020.140426.
Mousavi, A., Sowlat, M.H., Lovett, C., Rauber, M., Szidat, S., Boffi, R., Borgini, A., De Marco, C., Ruprecht, A.A., Sioutas, C., 2019. Source apportionment of black carbon (BC) from fossil fuel and biomass burning in metropolitan Milan, Italy. Atmos. Environ. 203, 252–261. https://doi.org/10.1016/j.atmosenv.2019.02.009.
Nakada, L.Y.K., Urban, R.C., 2020. COVID-19 pandemic: impacts on the air quality during the partial lockdown in São Paulo state, Brazil. Sci. Total Environ. 730, 139087 https://doi.org/10.1016/j.scitotenv.2020.139087.
Neykova, R., Hristova, E., 2020. Backward trajectories and cluster analyses for study of PM. Bulg. J. Meteorol. Hydrol. 24 (2), 66–83.
(n.d.-a) OMSZ. Climate of Hungary - general characteristics, from. https://www.met.hu/en/eghajlat/magyarorszag_eghajlata/altalanos_eghajlati_jellemzes/altalanos_leiras/. (Accessed 1 June 2023).
OMSZ. Hungarian air quality Network (n.d.-b). https://legszennyezettseg.met.hu/.
OMSZ. Meteorológiai adattár (n.d.-c). https://odp.met.hu/. (Accessed 10 August 2023).
Paatero, P., Tapper, U., 1994. Positive matrix factorization: a non-negative factor model with optimal utilization of error estimates of data values. Environmetrics 5 (2), 111–126. https://doi.org/10.1002/env.3170050203.
Pásztor, L., Laborczi, A., Bakacsi, Z., Szabó, J., Illés, G., 2018. Compilation of a national soil-type map for Hungary by sequential classification methods. Geoderma 311, 93–108. https://doi.org/10.1016/j.geoderma.2017.04.018.
Pérez, C., Haustein, K., Janjic, Z., Jorba, O., Huneeus, N., Baldasano, J.M., Black, T., Basart, S., Nickovic, S., Miller, R.L., Perlwitz, J.P., Schulz, M., Thomson, M., 2011. Atmospheric dust modeling from meso to global scales with the online NMMB/BSC-Dust model – Part 1: model description, annual simulations and evaluation. Atmos. Chem. Phys. 11 (24), 13001–13027. https://doi.org/10.5194/acp-11-13001-2011.
Pérez Velasco, R., Jarosińska, D., 2022. Update of the WHO global air quality guidelines: systematic reviews – an introduction. Environ. Int. 170, 107556 https://doi.org/10.1016/j.envint.2022.107556.
Putaud, J.-P., Pisoni, E., Mangold, A., Hueglin, C., Sciare, J., Pikridas, M., Savvides, C., Ondracek, J., Mbengue, S., Wiedensohler, A., Weinhold, K., Merkel, M., Poulain, L., van Pinxteren, D., Herrmann, H., Massling, A., Nordstroem, C., Alastuey, A., Reche, C., et al., 2023. Impact of 2020 COVID-19 lockdowns on particulate air pollution across Europe. Atmos. Chem. Phys. 23 (17), 10145–10161. https://doi.org/10.5194/acp-23-10145-2023.
Rajesh, T.A., Ramachandran, S., 2017. Characteristics and source apportionment of black carbon aerosols over an urban site. Environ. Sci. Pollut. Control Ser. 24 (9), 8411–8424. https://doi.org/10.1007/s11356-017-8453-3.
Rajta, I., Vajda, I., Gyürky, Gy, Csedreki, L., Kiss, Á.Z., Biri, S., van Oosterhout, H.A.P., Podaru, N.C., Mous, D.J.W., 2018. Accelerator characterization of the new ion beam facility at MTA Atomki in Debrecen, Hungary. Nucl. Instrum. Methods Phys. Res. Sect. A Accel. Spectrom. Detect. Assoc. Equip. 880, 125–130. https://doi.org/10.1016/j.nima.2017.10.073.
Rys, A., Samek, L., Stegowski, Z., Styszko, K., 2022. Comparison of concentrations of chemical species and emission sources PM2.5 before pandemic and during pandemic in Krakow, Poland. Sci. Rep. 12 (1), 16481 https://doi.org/10.1038/s41598-022-21012-x.
Salma, I., Vasanits-Zsigrai, A., Machon, A., Varga, T., Major, I., Gergely, V., Molnár, M., 2020a. Fossil fuel combustion, biomass burning and biogenic sources of fine carbonaceous aerosol in the Carpathian Basin. Atmos. Chem. Phys. 20 (7), 4295–4312. https://doi.org/10.5194/acp-20-4295-2020.
Salma, I., Vörösmarty, M., Gyöngyösi, A.Z., Thén, W., Weidinger, T., 2020b. What can we learn about urban air quality with regard to the first outbreak of the COVID-19 pandemic? A case study from central Europe. Atmos. Chem. Phys. 20 (24), 15725–15742. https://doi.org/10.5194/acp-20-15725-2020.
Samaké, A., Bonin, A., Jaffrezo, J.-L., Taberlet, P., Weber, S., Uzu, G., Jacob, V., Conil, S., Martins, J.M.F., 2020. High levels of primary biogenic organic aerosols are driven by only a few plant-associated microbial taxa. Atmos. Chem. Phys. 20 (9), 5609–5628. https://doi.org/10.5194/acp-20-5609-2020.
Sokhi, R.S., Singh, V., Querol, X., Finardi, S., Targino, A.C., Andrade, M. de F., Pavlovic, R., Garland, R.M., Massagué, J., Kong, S., Baklanov, A., Ren, L., Tarasova, O., Carmichael, G., Peuch, V.-H., Anand, V., Arbilla, G., Badali, K., Beig, G., et al., 2021. A global observational analysis to understand changes in air quality during exceptionally low anthropogenic emission conditions. Environ. Int. 157, 106818 https://doi.org/10.1016/j.envint.2021.106818.
Squizzato, S., Masiol, M., 2015. Application of meteorology-based methods to determine local and external contributions to particulate matter pollution: a case study in Venice (Italy). Atmos. Environ. 119, 69–81. https://doi.org/10.1016/j.atmosenv.2015.08.026.
Stein, A.F., Draxler, R.R., Rolph, G.D., Stunder, B.J.B., Cohen, M.D., Ngan, F., 2015. NOAA's HYSPLIT atmospheric transport and dispersion modeling System. Bull. Am. Meteorol. Soc. 96 (12), 2059–2077. https://doi.org/10.1175/BAMS-D-14-00110.1.
Szidat, S., Jenk, T.M., Synal, H., Kalberer, M., Wacker, L., Hajdas, I., Kasper-Giebl, A., Baltensperger, U., 2006. Contributions of fossil fuel, biomass-burning, and biogenic emissions to carbonaceous aerosols in Zurich as traced by ^{14}C. J. Geophys. Res. Atmos. 111 (D7) https://doi.org/10.1029/2005JD006590.
Urban, R.C., Lima-Souza, M., Caetano-Silva, L., Queiroz, M.E.C., Nogueira, R.F.P., Allen, A.G., Cardoso, A.A., Held, G., Campos, M.L.A.M., 2012. Use of levoglucosan, potassium, and water-soluble organic carbon to characterize the origins of biomass-burning aerosols. Atmos. Environ. 61, 562–569. https://doi.org/10.1016/j.atmosenv.2012.07.082.
Vadrevu, K.P., Eaturu, A., Biswas, S., Lasko, K., Sahu, S., Garg, J.K., Justice, C., 2020. Spatial and temporal variations of air pollution over 41 cities of India during the COVID-19 lockdown period. Sci. Rep. 10 (1), 16574 https://doi.org/10.1038/s41598-020-72271-5.
Varga-Balogh, A., Leelőssy, Á., Mészáros, R., 2021. Effects of COVID-induced mobility restrictions and weather conditions on air quality in Hungary. Atmosphere 12 (5), 561. https://doi.org/10.3390/atmos12050561.
World Health Organization, 2021. WHO Global Air Quality Guidelines: Particulate Matter (PM2.5 and PM10), Ozone, Nitrogen Dioxide, Sulfur Dioxide and Carbon Monoxide. World Health Organization. https://apps.who.int/iris/handle/10665/345329.
Yao, X., Lau, A.P.S., Fang, M., Chan, C.K., Hu, M., 2003. Size distributions and formation of ionic species in atmospheric particulate pollutants in Beijing, China: 1—inorganic ions. Atmos. Environ. 37 (21), 2991–3000. https://doi.org/10.1016/S1352-2310(03)00255-3.